The role of an interneuron in a chemotaxis circuit of C. elegans is determined by EGL-4/PKG that mediates integration of sensory signals

日野, 喬央

出版情報：九州大学, 2021, 博士（理学）, 課程博士
バージョン：
権利関係：

主論文

The role of an interneuron in a chemotaxis circuit of *C. elegans* is determined by

EGL-4/PKG that mediates integration of sensory signals

日野　喬央

Abstract

Interneurons, innervated by multiple sensory neurons, need to integrate information from these sensory neurons and respond to sensory stimuli adequately. Mechanisms how sensory information is integrated to form responses of interneurons are not fully understood. In *Caenorhabditis elegans*, loss-of-function mutations of *egl-4*, which encodes a cGMP-dependent protein kinase (PKG), cause a defect in chemotaxis to odorants. My genetic and imaging analyses revealed that the response property of AIY interneuron to an odorant is reversed in the *egl-4* mutant, while the responses of two upstream olfactory neurons, AWA and AWC, are largely unchanged. Cell-ablation experiments show that AIY in the *egl-4* mutant functions to suppress chemotaxis. Furthermore, the reversal of AIY response occurs only in the presence of sensory signals from both AWA and AWC. These results suggest that sensory signals are inadequately integrated in the *egl-4* mutant. I also show that *egl-4* expression in AWA and another sensory neuron prevents the reversed AIY response and restores chemotaxis in the *egl-4* mutants. I propose that EGL-4/PKG, by suppressing aberrant integration of signals from olfactory neurons, converts the response property of an interneuron to olfactory stimuli and maintains the role of the

interneuron in the circuit to execute chemotactic behavior.

Introduction

Sensory stimuli are detected by sensory neurons and elicit neuronal responses. In hard-wired neural circuitry, a sensory response to a stimulus generally elicits a certain pattern of response in downstream neurons. However, accumulating evidence demonstrates that the same pattern of sensory response is capable of eliciting different response patterns in a downstream neuron, thereby evoking different behavioral outputs (Barnhart et al., 2018; Gordus et al., 2015; Guillermin et al., 2017; Hawk et al., 2018; Jin et al., 2021; Nakano et al., 2020). For example, in the nematode, *Caenorhabditis elegans*, a CO_2-sensing neuron, BAG, is activated by increased levels of CO_2 and the activation elicits excitatory or inhibitory responses in a downstream interneuron, AIY, depending on the past experience of the animal (Guillermin et al., 2017). The opposing AIY responses drive the opposing behavioral outputs, attraction to and repulsion from CO_2. Thus, the relationship between the sensory neuron and the interneuron determines the valence of the sensory cue and seems to play a fundamental role in adaptation to environmental changes (Guillermin et al., 2017). However, the mechanisms by which sensory responses with the same properties can elicit distinct responses in downstream neurons are not fully

understood. Previous studies suggested presynaptic mechanisms by which a single sensory neuron can send different signals to a certain downstream interneuron (Nakano et al., 2020; Oda et al., 2011; Ohno et al., 2017). In the natural environment, sensory cues such as food are composed of multiple constituents that simultaneously activate multiple sensory neurons. When multiple sensory neurons are activated by a sensory cue, it is also unclear how sensory neuronal activities are integrated and elicit the response of downstream interneurons to regulate behavior.

Functional regulation of an interneuron by its upstream sensory neuron can be examined in detail in the *C. elegans* nervous system, which is composed of 302 neurons and whose inter-neuronal connections are fully elucidated (White et al., 1986). In *C. elegans* olfactory circuitry, two pairs of olfactory neurons called AWA and AWC, which express various olfactory receptors, are mainly responsible for detecting attractive odorants (Bargmann et al., 1993; Colosimo et al., 2004; Lesch and Bargmann, 2010; Sengupta et al., 1996; Troemel et al., 1999). These olfactory neurons innervate several interneurons that play important roles in regulating the animal's behavior (Chalasani et al., 2010, 2007; Itskovits et al., 2018; Larsch et al., 2013). Through this olfactory circuitry,

animals exhibit chemotaxis to various odorants, although AWA and AWC show distinct properties in sensory responses. In response to attractive odorants, AWA is activated by the addition of odorant (Shinkai et al., 2011), while AWC is suppressed by the addition of odorant and is activated by the removal of odorant (Chalasani et al., 2007). AIY interneuron, which is directly innervated by AWA and AWC, is activated by the addition of odorant sensed by AWA and AWC, and this activation induces forward movement of animals (Chalasani et al., 2010; Itskovits et al., 2018; Kocabas et al., 2012). Thus, AWA and AWC are thought to transmit excitatory and inhibitory signals to AIY, respectively. Because odorant addition activates AIY and the AIY activation induces forward movement of animals, AIY is considered to promote chemotaxis. Although AIY function is defined by innately programmed signal transmission, the function of AIY in chemotaxis may be dynamically regulated, as in the AIY function in CO_2 sensing (Chalasani et al., 2007; Guillermin et al., 2017).

Here, I show that loss-of-function mutations in *egl-4*, which encodes a *C. elegans* homologue of cGMP-dependent protein kinase (PKG), convert the response properties of AIY interneuron to odorant stimuli. I found that AIY ablation in the *egl-4* mutant improves chemotaxis towards a specific odorant.

AWA and AWC in the *egl-4* mutant, as well as in wild-type animals, can be activated by odorant addition and removal, respectively, whereas AIY in the *egl-4* mutant is activated by removal of odorant instead of by addition of odorant. The opposite activation of AIY is elicited only when signals from both AWA and AWC are present. These results suggest that EGL-4/PKG mediates the proper integration of signals from AWA and AWC to regulate the AIY response property, and thereby makes the role of AIY not to be suppressive in chemotaxis circuit of *C. elegans*.

Results

Primary sensory responses of AWA and AWC olfactory neurons are not reduced in the *egl-4* mutant

Mutations in *egl-4* cause pleiotropic phenotypes, including an egg-laying defect, abnormal dauer formation, a larger body size, increased roaming behavior, defective nociceptive behavior, and defective adaptation to odorants (Daniels et al., 2000; Fujiwara et al., 2002; Krzyzanowski et al., 2013; L'Etoile et al., 2002; Trent et al., 1983). Furthermore, *egl-4* mutants exhibit defects in chemotaxis to a subset of odorants (Daniels et al., 2000), although it is not clear how EGL-4/PKG functions in regulating chemotaxis. To analyze EGL-4 function in chemotaxis, I measured chemotaxis to a wide range of concentrations of the attractive odorants, diacetyl (diluted to 10^{-3}, 10^{-4} and 10^{-5}, which is equivalent to 11.5 mM, 1.15mM and 115 μM, respectively) and isoamyl alcohol (diluted to 10^{-3}, 10^{-4} and 10^{-5}, which is equivalent to 9 mM, 900 μM and 90 μM, respectively) (Figure 1*A, B*). For this analysis, I used two possible null alleles of *egl-4*, *ky185* and *n478*, which have a 0.8 kb-deletion in the coding region and a missense mutation in the conserved amino acid of the kinase domain, respectively (Fujiwara et al., 2002). Consistent with previous results (Daniels et al., 2000),

the *egl-4* mutants showed decreased chemotaxis to both odorants over wide concentration ranges (Figure 1*A* and 1*B*).

C. elegans senses attractive odorants mainly through AWA or AWC olfactory neurons (Bargmann et al., 1993). To examine if the olfactory responses of these neurons are impaired in the *egl-4* mutant, I analyzed the sensory responses to the odorants using the genetically encoded Ca^{2+} indicator, Yellow Cameleon (Nagai et al., 2004). In wild-type animals, the intracellular Ca^{2+} level transiently increased in AWA immediately after addition of diacetyl (Figure 1*C*), as previously reported (Fujiwara et al., 2016; Shinkai et al., 2011). In the *egl-4* mutant, AWA responses to addition of wide range of concentrations of diacetyl were comparable to those of wild-type animals (Figure 1*C*), although the response to 10^{-7} diacetyl was slightly smaller than wild type. This result suggests that the AWA sensory response to diacetyl was not affected in the *egl-4* mutant. Consistent with this result, the expression level of a diacetyl receptor, ODR-10, in AWA of the *egl-4* mutant was similar to that in wild-type animals, as determined by GFP-tagged construct quantification (Figure S1). Sensory responses of AWC of the *egl-4* mutant were analyzed by Shota Hirai. AWC of wild-type animals showed transient Ca^{2+} increase at removal of diacetyl (Figure

1*D*), as previously described (Chalasani et al., 2007). In AWC of the *egl-4* mutant, the Ca^{2+} increase at removal of a high concentration of diacetyl was indistinguishable from that in the wild type, although the Ca^{2+} increase in response to removal of a low concentration of diacetyl was larger than that in the wild type (Figure 1*D*). These results indicate that primary olfactory responses of AWA and AWC to diacetyl are not diminished in the *egl-4* mutant, whereas AWC responses are rather enhanced. These results suggested that EGL-4 is important for the regulation of chemotaxis in a pathway downstream of the olfactory neuron Ca^{2+} responses.

AIY interneuron of the *egl-4* mutant acts to suppress chemotaxis to diacetyl but not to isoamyl alcohol

AWA and AWC olfactory neurons make synapses to several interneurons, including AIA, AIB and AIY, which play important roles in directing chemotaxis (Gray et al., 2005; White et al., 1986). To examine if the *egl-4* mutation affects chemotactic behavior through these interneurons, I analyzed chemotaxis to odorants in animals missing one of these interneurons. First, I ablated AIA in wild-type animals by cell-specific expression of caspase and confirmed that the

AIA ablation decreased chemotaxis to diacetyl (Figure 2*A*) (Fujiwara et al., 2016; Larsch et al., 2015). Thus, the function of AIA is important for chemotaxis to diacetyl. AIA ablation in *egl-4(ky185)* mutant animals also caused a similar decrease in chemotaxis, suggesting that EGL-4 is not required for the AIA function (Figure 2*A*). Next, I analyzed animals in which AIB was ablated by caspase. In wild-type animals, AIB ablation caused decreased chemotaxis to diacetyl as shown previously (Fujiwara et al., 2016). Thus, AIB function is also important for chemotaxis. In the *egl-4 (ky185)* mutant animals, however, chemotaxis to diacetyl was not further decreased by the ablation of AIB (Figure 2*B*), suggesting that AIB in *egl-4* is not functioning for chemotaxis and that EGL-4 is required for the AIB function. Finally, I analyzed animals of which AIY was ablated by caspase. In wild-type animals, I did not detect the effect of AIY ablation on chemotaxis at least in our assay condition. On the contrary, in *egl-4 (ky185)* mutant animals, the ablation of AIY significantly improved chemotaxis to wide range of concentrations of diacetyl (Figure 2*C*). To confirm the effect of the loss of AIY, I used a *ttx-3* mutant strain, in which the terminal differentiation of AIY and several other neurons is impaired and functional AIY is missing (Altun et al., 2008; Hobert et al., 1997). The chemotaxis of *ttx-3(ks5)* mutant

was comparable to that of wild type (Figure S2*A*). However, the *egl-4(ky185); ttx-3(ks5)* double mutant showed a higher chemotaxis index than the *egl-4(ky185)* single mutant (Figure S2*A*). Furthermore, in the *egl-4; ttx-3* double mutant, expression of the *ttx-3* gene only in AIY [by trimmed *ttx-3* promoter (Hobert et al., 1997)] decreased the chemotaxis index to the level of the *egl-4* mutant, restoring the phenotype of *egl-4* (Figure S2*B*). Taken together, the absence of a functional AIY interneuron improves chemotaxis of the *egl-4* mutant, indicating that, in the absence of EGL-4, AIY acts to suppress chemotaxis to diacetyl.

Next, I examined if, in the *egl-4* mutant, AIY also suppresses chemotaxis to another attractive odorant, isoamyl alcohol. AIY ablation by caspase did not affect chemotaxis to isoamyl alcohol in the wild type nor in the *egl-4* mutant (Figure2*D*), indicating that, in the *egl-4* mutant, AIY suppresses chemotaxis specifically to diacetyl, but not to isoamyl alcohol.

AIY in the *egl-4* mutant shows reversed Ca^{2+} response to diacetyl stimuli, but not to isoamyl alcohol

How does AIY in the *egl-4* mutant respond to odorant stimuli, if AIY acts to

suppress chemotaxis? And how does EGL-4 in the wild type prevent AIY from suppressing chemotaxis? To answer these questions, I first analyzed the Ca^{2+} responses in AIY to diacetyl stimuli. In wild-type animals, addition of diacetyl (diluted to 10^{-7}) induced an increase of intracellular Ca^{2+} in AIY, while removal of diacetyl caused a gradual decrease of Ca^{2+} (Figure 3*A*, Table S1). In the *egl-4 (ky185)* mutant, the Ca^{2+} responses in AIY were distinct from those in the wild type; addition of diacetyl elicited a temporal Ca^{2+} decrease that quickly returned to the basal level and was followed by fluctuated Ca^{2+} changes (Figure 3*A*, Table S1). Furthermore, the removal of odorant induced an increase of Ca^{2+} in AIY (Figure 3*A*). Similar AIY responses were also observed when high concentration diacetyl (diluted to 10^{-5}) was used as the stimulus (Figure S3, Table S1). Thus, in the *egl-4* mutant, the addition and removal of diacetyl induced a transient decrease and an increase of intracellular Ca^{2+} in AIY, respectively. These response properties are opposite to those in wild-type animals, and AIY responses to diacetyl can be considered as reversed in the *egl-4* mutant.

Next, I analyzed AIY responses to isoamyl alcohol. Because AIY ablation did not improve chemotaxis of the *egl-4* mutant to isoamyl alcohol (Figure 2*D*), I expected that the Ca^{2+} responses of AIY to isoamyl alcohol would not be reversed.

In the wild type, AIY response to isoamyl alcohol (diluted to 10^{-4}) was similar to the response to diacetyl (Figure 3*B*). In the *egl-4(ky185)* mutant, as in the wild type, addition and removal of isoamyl alcohol induced Ca^{2+} increase and decrease in AIY, respectively, although the increase of intracellular Ca^{2+} was declined faster than in the wild type. Thus, AIY in the *egl-4* mutant showed a reversed Ca^{2+} response specifically to diacetyl, but not to isoamyl alcohol. Taken together with the AIY ablation experiments, these results suggest that AIY in the *egl-4* mutant suppresses chemotaxis to diacetyl by responding to stimuli with Ca^{2+} changes opposite to those of the wild type. Because activation of AIY promotes forward movement, Ca^{2+} increase in response to diacetyl addition is considered to facilitate attraction of wild-type animals to diacetyl (Gray et al., 2005; Li et al., 2014). On the other hand, in the *egl-4* mutant, Ca^{2+} increase in AIY at diacetyl removal may keep animals away from the odorant source and thereby suppress chemotaxis.

Enhanced AWC response does not reverse the AIY response

As shown in Figure 1*D*, in the *egl-4* mutant, removal of low concentration diacetyl induced a larger Ca^{2+} increase in AWC than in the wild type. It is possible that this enhanced AWC sensory response elicits the reversed response

in the *egl-4* mutant AIY. To examine this possibility, I analyzed AIY responses when AWC Ca^{2+} responses were enhanced. Chalasani et al. reported that prolonged application of odorant induces a larger Ca^{2+} increase at the removal of the odorant (Chalasani et al., 2007). Consistently, I found that, in wild-type animals, longer duration (5 min) of diacetyl exposure induced larger Ca^{2+} increases in AWC at odor removal than a shorter, 1 min, exposure (Figure 4*A*). Next, I measured AIY Ca^{2+} responses to prolonged diacetyl application in wild-type animals, and found that prolonged application still induced the Ca^{2+} decrease in AIY at odor removal, and did not mimic AIY of the *egl-4* mutant, which shows Ca^{2+} increase at odor removal (Figure 4*B*). These results suggest that the enhanced AWC response at diacetyl removal in the *egl-4* mutant cannot explain the reversed AIY responses to diacetyl observed in *egl-4.*

The reversed AIY response to diacetyl in the *egl-4* mutant is induced by the integration of signals from AWA and AWC olfactory neurons

Both of AWA and AWC olfactory neurons, which are the major sensory neurons of diacetyl, directly innervate AIY and elicit AIY olfactory responses (Chalasani et al., 2007; Itskovits et al., 2018), suggesting that AWA and/or AWC regulate

the AIY response properties. To explore how the reversed AIY responses to diacetyl are evoked in the *egl-4* mutant, I measured AIY responses in animals missing functional AWC or AWA neurons using animals with a mutation in *ceh-36* or *odr-7*, which encode proteins required for normal differentiation of AWC and AWA, respectively (Koga and Ohshima, 2004; Lanjuin et al., 2003; Sengupta et al., 1994). In the *ceh-36(ks86)* mutant, in which functional AWC was absent, addition and removal of diacetyl (diluted to 10^{-7}) evoked Ca^{2+} increase and decrease in AIY, respectively (Figure 5*B*, Table S1). These responses are comparable to those in wild-type animals, suggesting that the AIY responses to diacetyl (10^{-7}) stimulation largely depend on AWA inputs but not on AWC inputs (Figure 5*A*, 5*B*). Interestingly, when functional AWC was removed from the *egl-4(ky185)* mutant [in *egl-4(ky185); ceh-36(ks86)*], AIY responses became similar to those of the *ceh-36(ks86)* mutant and wild-type animals (Figure 5*B*). In *egl-4(ky185); ceh-36(ks86)*, neither the Ca^{2+} decrease at diacetyl addition nor the Ca^{2+} increase at diacetyl removal were observed, being different from the *egl-4(ky185)* single mutant (Figure 5*A*, 5*B*). I confirmed the effect of AWC loss, by ablating AWC and also AWB in the *egl-4(ky185)* mutant by expressing caspase under the *gcy-10* promoter (Yu et al., 1997). With the

strain, I obtained a consistent result (Figure S4). These results suggest that AIY can be activated normally in the *egl-4* mutant without AWC probably through AWA, and that AWC is required for the conversion of AIY response properties observed in the *egl-4* mutant. In the *odr-7(ky4)* mutant in which functional AWA was absent, addition of diacetyl (diluted to 10^{-7}) evoked Ca^{2+} increase in AIY similarly to that in wild-type AIY, but the size of the Ca^{2+} increase was smaller than that in the wild type (Figure 5*A*, 5*C*, Table S1). This is consistent with the notion that AIY responses to diacetyl (10^{-7}) stimulation largely depend on AWA inputs. Interestingly when functional AWA was removed from the *egl-4(ky185)* mutant [in *egl-4(ky185); odr-7(ky4)*], neither Ca^{2+} decrease at diacetyl addition nor Ca^{2+} increase at diacetyl removal were observed, being different from the response of the *egl-4(ky185)* single mutant (Figure 5*C*). In the *egl-4; odr-7* double mutant, I instead observed a Ca^{2+} increase during diacetyl application (Figure 5*C*, Table S1). Although the Ca^{2+} increase in *egl-4; odr-7* appeared to be larger than the Ca^{2+} increase in the *odr-7 (ky4)* single mutant (Figure 5*C*), the difference was not significant even when compared the entire odor-application period ($p=0.127$, two-tailed t-test). These results suggest that AWA is also required for conversion of the AIY response properties

observed in the *egl-4* mutant. Taken together, our results suggest that both AWA and AWC olfactory neurons are required for the change in the AIY response properties. This leads to a model that, in the *egl-4* mutant, integration of signals from AWA and AWC olfactory neurons induces the reversed AIY response to diacetyl (Figure S5). In this model, EGL-4 in wild-type animals may inhibit the integration of signals from AWA and AWC to prevent reversal of AIY response properties, and thereby promotes the attractive behavior to diacetyl.

As shown in Figure *5B,* the *egl-4; ceh-36* mutant showed AIY response that is not reversed but comparable to the response in *ceh-36* single mutant. If the reversed AIY response actually acts to suppress chemotaxis, I expected that the *egl-4; ceh-36* mutant would not show lower chemotaxis than the *ceh-36* single mutant. To examine this possibility, I compared chemotaxis of the *ceh-36* and the *egl-4; ceh-36* mutants (Figure S6). The *ceh-36* mutant showed decreased chemotaxis to high concentration of diacetyl (10^{-2}) (Figure S6), being consistent with the AWC function to sense high concentration of diacetyl (Chou et al., 2001). Contrary to the expectation, *egl-4(ky185); ceh-36(ks86)* animals showed lower chemotaxis than *ceh-36(ks86)* to diacetyl over a wide range of concentrations (Figure S6). Thus, the *egl-4* mutation in the *ceh-36* mutant

background, even if AIY responds normally to diacetyl, still decreases chemotaxis. I speculate that this chemotaxis reduction may be due to effects of the *egl-4* mutation on other neurons, which may include AIB as EGL-4 is also required for the AIB function in chemotaxis (Figure 2*B*).

EGL-4 acts in AWA and ASI sensory neurons to prevent AIY from eliciting the reversed response to diacetyl and to promote chemotaxis to diacetyl

egl-4 is expressed in many head neurons and in the body wall muscles (Fujiwara et al., 2002). EGL-4 regulates various functions in distinct cell types; expression of *egl-4* in multiple sensory neurons, including URX, PQR, and AQR, is important for body size regulation (Mok et al., 2011), expression in AWC olfactory neuron is important for olfactory adaptation (L'Etoile et al., 2002), and expression in ASH sensory neuron is important for nociceptive behavior (Krzyzanowski et al., 2013). I asked in which cells EGL-4 acts to control chemotaxis and the olfactory response of AIY. I made an *egl-4(ky185)* mutant expressing wild-type *egl-4* under various cell-specific promoters to analyze chemotaxis to diacetyl. *egl-4* expression driven by an original promoter (*egl-4.ap*) and a pan-neuronal promoter (*H20p*) (Shioi et al., 2001) restored the

chemotaxis of the *egl-4* mutant (Figure 6*A*). Furthermore, *egl-4* expression driven by the *tax-4* promoter restored the chemotaxis of the *egl-4* mutant (Figure 6*A*). The *tax-4* promoter drives expression in 10 pairs of sensory neurons (Komatsu et al., 1996) (Figure 6*C*). I tried to narrow down the cells sufficient for the restoration of chemotaxis. *egl-4* expression in AIY (by *ttx-3p*), AWC (by *ceh-36p*) or AWA (by *odr-10p*) (Ferkey et al., 2007; Sengupta et al., 1996) failed to restore chemotaxis (Figure 6*A, B*). *egl-4* expression in both AWA and AWC (by a combination of *odr-10p* and *gcy-10p*) also failed to restore chemotaxis (Figure 6*A, B*). However, *egl-4* expression in AWA and ASI (by the *gpa-4p*) (Kim et al., 2005) restored chemotaxis although *egl-4* expression solely in ASI (by *daf-7p*) did not (Figure 6*B*). Furthermore, *egl-4* expression in AWA and ASI using a combination of *odr-10p* and *daf-7p* restored chemotaxis (Figure 6*B*). These results suggest that EGL-4/PKG acts in two pairs of sensory neurons, AWA and ASI, to regulate chemotaxis to diacetyl.

Next, I examined whether the *egl-4* expression in AWA and ASI in the *egl-4(ky185)* mutant restores the Ca^{2+} responses of AIY. Expression of the wild-type *egl-4* gene in AWA and ASI (using *gpa-4p*) or in AWA (using *odr-10p*) did not change the AIY response of the *egl-4* mutant at odor addition; I still

observed slight Ca^{2+} decreases after addition of diacetyl (Figure 6*D*). However, with *egl-4* expression in both AWA and ASI (using *gpa-4p*), the Ca^{2+} increase at removal of diacetyl was significantly diminished, while *egl-4* expression solely in AWA (using *odr-10p*) did not have such an effect (Figure 6*D*). These results indicate that the expression of *egl-4* in both AWA and ASI is sufficient to decrease the AIY activation at diacetyl removal and thereby facilitates attractive behavior toward diacetyl.

Since EGL-4 is known to function in developmental regulation as well as in sensory perception, EGL-4 could function during development or at adult stage to regulate chemotaxis to diacetyl. To determine when EGL-4 acts to regulate chemotaxis to diacetyl, I generated *egl-4(ky185)* and wild-type animals expressing wild-type *egl-4* under the control of a heat shock promoter (*hsp16.2*) (Stringham et al., 1992). Adult animals were exposed to a heat shock (33 ℃, 2 hr) and their chemotactic ability to diacetyl after a 2 hr recovery was measured. The heat shock did not affect the chemotaxis of wild-type animals nor *egl-4* mutant animals without the transgene (Figure 6*E*). However, in the *egl-4* mutant animals with the transgene, the heat shock improved chemotaxis to diacetyl (Figure 6*E*). This result indicates that *egl-4* expression in the adult is sufficient

for its function in chemotaxis to diacetyl.

AIB of the *egl-4* mutant showed decreased response to diacetyl

I also showed that AIB in *egl-4* is not functioning for chemotaxis to diacetyl (Figure 2*B*). Olfactory response of AIB might be impaired in the *egl-4* mutant. I measured AIB Ca^{2+} response to diacetyl in the *egl-4* mutant. In wild-type animals, addition of diacetyl (diluted to 10^{-7}) induced a decrease of intracellular Ca^{2+} in AIB, while removal of diacetyl caused a gradual increase of Ca^{2+}, as previously described (Fujiwara et al., 2016). In the *egl-4* mutant, the level of AIB suppression by diacetyl addition was smaller than wild type (Figure 7). This result suggests that EGL-4 is required for normal olfactory response of AIB. Since EGL-4 acts in AWA and ASI sensory neurons to regulate the AIY response, AIB response might be also regulated by EGL-4 in these neurons. To examine this possibility, I expressed *egl-4* in AWA and ASI sensory neurons in the *egl-4* mutant and measured AIB response. The *egl-4* expression in AWA and ASI did not affect the AIB response (Figure 7). This result suggests that EGL-4 in neurons other than AWA and ASI is required for the regulation of AIB response.

Discussion

The role of AIY in chemotaxis is controlled by EGL-4/PKG

To achieve effective chemotaxis to attractive odorants, worms should move forward when they detect an increased concentration of an odorant, while they should turn or change direction when they detect a decrease in the concentration of an odorant. The AIY interneuron is activated by addition of attractive odorants and AIY activation promotes forward movement of animals (Kocabas et al., 2012; Li et al., 2014); therefore, AIY has been considered to promote chemotaxis to attractive odorants. Actually an mutant with a defect in AIY differentiation was shown to exhibit a certain chemotaxis defect (Tsalik and Hobert, 2003). In this study, I showed that ablation of AIY restores the chemotaxis to diacetyl in the *egl-4* mutant, suggesting that AIY in the *egl-4* mutant acts to suppress chemotaxis. Consistent with this, in the *egl-4* mutant, diacetyl removal but not diacetyl addition induces Ca^{2+} increase in AIY (Figure 3*A*). Thus, in the *egl-4* mutant, AIY seems to promote forward movement with a decrease in odorant concentration and thereby keeps animals away from the odorant source. Based on these results, I propose that EGL-4 cGMP-dependent protein kinase (PKG) regulates the response properties of AIY to diacetyl and

maintains the AIY role not to be suppressive in chemotaxis circuit.

Diacetyl is an odor associated with food (Drider et al., 2004). Under what circumstances does EGL-4/PKG change the attractive behavior to diacetyl? I suppose that *C. elegans*, through EGL-4, may change the AIY role in chemotaxis to be suppressive when animals face an important event that should be prioritized over searching for food, such as avoiding dangers or finding mating partners, or when animals learn that an odorant has little benefit for them. In sensory neurons, change of neuronal role in chemotaxis was also reported by the analysis of guanylyl cyclase, *gcy-28* (Tsunozaki et al., 2008). GCY-28 acts in AWC olfactory neuron to modify the odorant response of the downstream interneuron, AIB, and converts the behavioral output from attraction to repulsion (Tsunozaki et al., 2008). It is interesting that the cGMP signaling components in sensory neurons, such as EGL-4/PKG and GCY-28/guanylyl cyclase, share roles with valence control of olfactory behavior. These mechanisms that allow flexible changes in response of downstream interneurons might be important for animals to quickly adapt to environmental changes.

Analysis of chemotaxis in cell-ablation lines showed that, in the *egl-4* mutant, the function of another interneuron, AIB, in chemotaxis to diacetyl was also

impaired (Figure 2*B*). Consistent with this result, olfactory response of AIB to diacetyl was decreased in the *egl-4* mutant (Figure 7). AIB response to diacetyl seems to be regulated by EGL-4/PKG acting in neurons rather than AWA and ASI sensory neurons. Thus, the function of AIB and AIY seems to be separately regulated by the EGL-4 in different neurons. I suppose that EGL-4 act in multiple neurons and these EGL-4 act in distinct aspects of physiologies to regulate chemotaxis. For example, I also showed that the *egl-4* mutant showed chemotactic defect to isoamyl alcohol, which was not due to the change of AIY response properties. This might be caused by impaired function of AIB or other neurons in the *egl-4* mutant. Because I used loss-of-functions mutant of the *egl-4*, it might be difficult to separately analyze the EGL-4 functions. Future research including cell specific knock down of *egl-4* may elucidate individual EGL-4 functions in multiple neurons for the regulation of chemotaxis.

The integration of signals from two olfactory neurons converts the properties of the AIY olfactory response

The change of AIY response properties in the *egl-4* mutant was only observed in the presence of both sensory signals from AWA and AWC (Figure 5). Although,

in the *egl-4* mutant, the AWC response to diacetyl is enhanced, this enhancement is not sufficient to elicit the reversed AIY response (Figure 4). Thus, the change of the AIY response properties seems to be regulated by the integration of AWA and AWC signals (Figure S5). However, the mechanism by which AIY response properties change is unclear. A reversed AIY olfactory response was also reported in a mutant of a glutamate-gated chloride channel, *glc-3* (Chalasani et al., 2007). In the wild type, AIY expresses GLC-3 and is tonically inhibited through GLC-3 by glutamate released from AWC. Odorant addition suppresses AWC and its glutamate release and, therefore, induces AIY activation (Chalasani et al., 2007; Ventimiglia and Bargmann, 2017). In the absence of GLC-3, AIY is not activated by the addition of odorant, but is instead activated by the removal of odorant (Chalasani et al., 2007). This result implicates that other neuronal transmission occurs and activates AIY at odorant removal whenever odorant addition fails to evoke activation in AIY. It is possible that, in the *egl-4* mutant, the integration of AWA and AWC signals prevents activation of AIY at odor addition, and this allows activation of AIY at odor removal, as in the *glc-3* mutant (Figure S5). Although the cellular and molecular bases of the integration process are still unknown, when EGL-4/PKG functions

in the sensory neurons, as discussed below, the integration may be inhibited, and thereby the AIY response properties are maintained as not to be suppressive in chemotaxis (Figure S5).

Interestingly, in contrast to diacetyl, to isoamyl alcohol, AIY in the *egl-4* mutant did not show a change in response properties and did not suppress chemotaxis. Thus, EGL-4 is required for olfactory responses in an odorant-specific manner. It is largely unknown how the *C. elegans* nervous system encodes information of various odorants and discriminates them. EGL-4/PKG may be involved in such discrimination of odorants.

EGL-4/PKG acts in AWA and ASI sensory neurons to control AIY olfactory responses and to regulate chemotaxis

I showed that *egl-4* expression in both AWA and ASI sensory neurons, but not individually, is sufficient to restore chemotaxis and to diminish the improper AIY activation at odorant removal, although the effect at diacetyl addition is ambiguous (Figure 6*A-D*). Furthermore, I showed that *egl-4* expression in the adult is sufficient to recover chemotaxis (Figure 6*E*), implicating that its role is not in development but in neural regulation. ASI is a sensory neuron that

responds to various stimuli, including food and pheromones, and is known to regulate many physiological processes by secreting extracellular signaling molecules, such as TGF-β (Bargmann and Horvitz, 1991; Calhoun et al., 2015; Ren et al., 1996; Schackwitz et al., 1996). Thus, EGL-4/PKG in ASI may affect the integration process of AWA and AWC signals according to environmental conditions, possibly through regulating secretion of extracellular signals (Figure S5). When EGL-4/PKG function is lost in either AWA or ASI, inappropriate integration of AWA and AWC signals would occur and that would induce the reversed response in AIY interneurons to diacetyl stimuli, as observed in the *egl-4* mutant (Figure S5).

The molecular targets of EGL-4/PKG involved in controlling the AIY response are unclear. EGL-4/PKG regulates sensory transduction by phosphorylating molecules involved in sensory signaling, such as cyclic nucleotide gated channels (TAX-2 and CNG-3) (L'Etoile et al., 2002; O'Halloran et al., 2017) and regulator of G protein signaling proteins (RGS-2, 3) (Krzyzanowski et al., 2013). Among them, *tax-2*, *cng-3* and *rgs-3* are expressed in ASI (Cho et al., 2004; Coburn and Bargmann, 1996; Ferkey et al., 2007), although their expression in AWA has not been reported. Thus, one possible

mechanism is that EGL-4/PKG regulates sensory transduction in ASI by phosphorylating these signaling molecules and the change in sensory transduction may eventually affect the integration of sensory signals. EGL-4/PKG is also known to regulate gene expression by phosphorylating the histone deacetylase, HDA-4, the transcription factor, MEF-2, and the HP1 homolog, HPL-2 (Juang et al., 2013; Lee et al., 2010; Van Der Linden et al., 2008). Thus, it is also possible that in AWA and ASI, EGL-4/PKG controls the expression of genes required to regulate the integration of sensory signals. Further studies will reveal the molecular mechanism of EGL-4/PKG function in AWA and ASI neurons.

Several studies have demonstrated that response properties of downstream interneurons can be changed by the presynaptic signaling cascade in upstream sensory neurons (Nakano et al., 2020; Oda et al., 2011; Ohno et al., 2017). Our results propose another mechanism whereby the integration of signals from multiple sensory neurons can change the response properties of their downstream interneuron. EGL-4/PKG mediates the integration of sensory signals and regulates the role of the interneuron in chemotaxis. Considering that natural stimuli, such as food, contain various volatile and soluble chemicals and

may stimulate multiple sensory neurons simultaneously, the sensory-integration-dependent regulation of the downstream response might be an effective way for *C. elegans* to flexibly adapt to environmental changes.

Experimental procedures

Strains and culture

The strains used in this study were: wild-type Bristol strain N2, *egl-4(ky185)*, *odr-7(ky4)*, *ceh-36(ks86)*, *egl-4(ky185); odr-7(ky4)*, *egl-4(ky185); ceh-36(ks86)*, *ttx-3(ks5)*, and *egl-4(ky185); ttx-3(ks5)*. All strains including transgenic lines are listed in Table S2. All strains were cultured on nematode growth medium (NGM) plates with *Escherichia coli* strain OP50 under standard conditions (Brenner, 1974). All strains were grown at 20 ℃. All animals used in this study were hermaphrodite.

Genetic cell ablation

For genetic cell ablation analyses, the strains JN578 *peIs578[npr-9p::casp1/npr-9p::venus/unc-122p::mCherry]* (AIB ablated strain), and JN580 *peIs580[ins-1(short)p::casp1/ins-1(short)p::venus/unc-122p::gfp]* (AIA ablated strain) were kindly provided by Y. Iino (The University of Tokyo). The strain *Is[odr-1::mCasp1.mec-4::gfp]* (AWB and AWC ablated strain) was kindly provided by T. Wakabayashi (Iwate University). For genetic AIY ablation, I generated *Ex[*trimmed *ttx-3p::cz::casp3/*trimmed *ttx-3p::casp3::nz/*trimmed

ttx-3p::rfp/lin-44p::gfp]. An 834 bp region within the *ttx-3* promoter (trimmed *ttx-3p*) [kindly provided by O. Hobert (Columbia University)], which drives expression specifically in AIY (Hobert et al., 1997), was fused to each subunit of mouse caspase, *cz::casp3* and *casp3::nz* (Chelur and Chalfie, 2007), and *rfp* using the Gateway cloning system (Thermo Fisher Scientific, Waltham, MA, USA). Trimmed *ttx-3p::cz::casp3* and trimmed *ttx-3p::casp3::nz* were injected at 100 ng/μl with trimmed *ttx-3p::rfp* (at 50 ng/μl) as a cell-ablation marker and *lin-44p::gfp* (at 15 ng/μl) as an injection marker. Cell-ablation in these transgenic lines was confirmed by examining for loss of cell-specific marker fluorescence. These chromosomal insertions (Is) and extrachromosomal arrays (Ex) were transferred to the *egl-4(ky185)* background by mating.

Calcium imaging

For calcium imaging analyses, the Gateway cloning system (Thermo Fisher Scientific) was used to express Yellow Cameleon 3.60 (YC3.60) or Yellow Cameleon 2.60 (YC2.60) (Nagai et al., 2004) under control of the *odr-10* promotor (Sengupta et al., 1996) for imaging AWA, the *odr-3* promotor (Roayaie et al., 1998) for imaging AWC, the *inx-1* promotor (Altun et al., 2009)

for imaging AIB and the trimmed *ttx-3* promotor (Hobert et al., 1997) for imaging AIY. The extrachromosomal arrays were transferred from the control background to each mutant used for imaging analysis by mating. Calcium imaging analyses were performed using a microfluidic olfactory chip, as described previously (Chronis et al., 2007). In brief, animals were trapped in the microfluidic device and the worm's nose was exposed to a stream of buffer. To apply a diacetyl or isoamyl alcohol stimulus, the stream was switched from buffer to diluted odorant. Fluorescence images of YFP and CFP were captured using an Axioplan 2 microscope (Zeiss, Oberkochen, Germany) equipped with a 40× objective and a 3CCD digital camera (C7780; Hamamatsu Photonics K.K., Shizuoka, Japan). All images were captured with an exposure time of 300 ms. I used AquaCosmos software (version 2.6; Hamamatsu Photonics K.K.) to analyze the average intensity of YFP and CFP fluorescence within the region of interest and calculated the YFP/CFP ratio (R) at each time point. The region of interest was set on an AWA, AWC or AIB cell body. For AIY imaging, the region of interest was set on an axon bulb in the axonal region entering the nerve ring. To analyze temporal ratio changes in AWA, AIB and AIY, I first calculated the basal YFP/CFP ratio ($R_{0(ON)}$) by averaging the YFP/CFP ratio during a 5 sec period

(or a 30 sec period for AIB) preceding odor addition for each recording. Then, the YFP/CFP ratio change ($R/R_{0(ON)}$) was obtained by dividing "R" by "$R_{0(ON)}$" at each time point. To analyze temporal ratio changes in AWC, I first calculated the basal YFP/CFP ratio ($R_{0(OFF)}$) by averaging the YFP/CFP ratio during a 5 sec period preceding odor removal. Then, the YFP/CFP ratio change ($R/R_{0(OFF)}$) was obtained by dividing "R" by "$R_{0(OFF)}$" at each time point. To quantify the size of ratio changes at odor addition in AWA, AIB and AIY, I calculated the average of "$R/R_{0(ON)}$" during the time period after starting odor application. The time periods used for quantification are indicated in each figure. To quantify the size of ratio changes at odor removal in AWC and AIY, the average of "$R/R_{0(OFF)}$" during the time period after odor removal was calculated. The time periods used for quantification are indicated in each figure. Sample sizes (n) indicate the number of tested worms.

Behavioral assays

Chemotaxis assays were performed as described previously (Bargmann et al., 1993). 100-200 washed adult animals were placed for each assay plate (9 cm). NaN_3 (an anesthetic) was used to capture worms at the odor and diluent area.

After 1 hr from onset of the assay, I manually counted the number of animals in each area that is 2 cm radius of odorant source or diluent source. And chemotaxis indices were calculated using the formula (#A-#B)/#all, where #A is the number of animals at the odorant area, #B is the number of animals at the diluent (ethanol) area, and #all is the total number of animals. The assays were performed on at least 2 different days. Sample size (n) indicates the number of assay plates.

Heat shock experiments

All animals for heat shock experiments were grown at 20 ℃ until the young adult stage. For heat shock (+) groups, young adult animals were incubated at 33 ℃ for 2 hr and then allowed to recover at room temperature for an additional 2 hr. For heat shock (-) groups, young adult animals were kept at room temperature for 4 hr. Animals were then used for chemotaxis assays.

Analysis of ODR-10 expression

For analysis of ODR-10 expression, *Ex[odr-10 tagged gfp/ttx-3p::rfp]* was used (Sengupta et al., 1996). This extrachromosomal array was transferred to the

egl-4(ky185) background by mating. After picking animals with RFP fluorescence (the injection marker), I observed ODR-10::GFP levels by fluorescence microscopy (×63) and classified expression into three categories: bright (clear cilium morphology was observed), faint (blurred cilium morphology was observed), and no expression.

DNA constructs and germline transformation for rescue experiments

To generate transgenic animals for *egl-4(ky185)* mutant rescue experiments, an *egl-4.a* cDNA (Fujiwara et al., 2002) was fused to promoters using the Gateway cloning system (Thermo Fisher Scientific). Promoters used were *H20p* (~2.7 kb) (Shioi et al., 2001), *tax-4p* (~3.0 kb) (Komatsu et al., 1996), *ceh-36p* (368 bp) (Lanjuin et al., 2003), *odr-10p* (~2.9 kb) (Sengupta et al., 1996), trimmed *ttx-3p* (834 bp) (Hobert et al., 1997), *gcy-10p* (~4.0 kb) (Yu et al., 1997), *gpa-4p* (~4.0 kb) (Kim et al., 2005), and *daf-7p* (~3.1 kb) (Schackwitz et al., 1996), *hsp-16.2p* (401 bp) (Bacaj and Shaham, 2007). To generate transgenic animals for rescue experiments of the *ttx-3(ks5)* mutant, a *ttx-3.a* cDNA [kindly provided by O. Hobert, (Columbia University)] was fused to the trimmed *ttx-3p* (834 bp) (Hobert et al., 1997) using the Gateway cloning system (Thermo Fisher

Scientific). The fusion gene was injected at a concentration of 30 ng/μl into *ttx-3(ks5)* mutant animal. To generate transgenic animals for chemotaxis assays or calcium imaging, *myo-3p::gfp* (10 ng/μl) or *lin-44p::gfp* (10 ng/μl), respectively, was co-injected as an injection maker with empty vector (60 ng/μl).

Acknowledgments

This work was supported by a Japan Society for the Promotion of Science (JSPS) Research Fellows (JP18J11948 to T.H.) and by JSPS KAKENHI (JP23370002, JP25115009, JP18H05135, JP17H06113, and JP19H03326 to T.I. and JP17K07503 to M.F.). I would like to express my appreciation to my supervisors Takeshi Ishihara and Manabi Fujiwara for their very informative guidance. I thank Hirai Shota for his support of my research. I also thank Yuichi Iino for JN578 (AIB ablated strain) and JN580 (AIA ablated strain), Tokumitsu Wakabayashi for the AWB and AWC ablated strain, Oliver Hobert for pOH22 and pOH443 plasmids, the Caenorhabditis Genetics Center for strains, and Noriko Sato for technical assistance.

References

Altun ZF, Chen B, Wang ZW, Hall DH. 2009. High resolution map of Caenorhabditis elegans gap junction proteins. *Dev Dyn* **238**:1936–1950. doi:10.1002/dvdy.22025

Bacaj T, Shaham S. 2007. Temporal control of cell-specific transgene expression in Caenorhabditis elegans. *Genetics* **176**:2651–2655. doi:10.1534/genetics.107.074369

Bargmann CI, Hartwieg E, Horvitz HR. 1993. Odorant-selective genes and neurons mediate olfaction in C. elegans. *Cell* **74**:515–527. doi:10.1016/0092-8674(93)80053-H

Bargmann CI, Horvitz HR. 1991. Control of larval development by chemosensory neurons in Caenorhabditis elegans. *Science (80-)* **251**:1243–1246. doi:10.1126/science.2006412

Barnhart EL, Wang IE, Wei H, Desplan C, Clandinin TR. 2018. Sequential Nonlinear Filtering of Local Motion Cues by Global Motion Circuits. *Neuron* **100**:229-243.e3. doi:10.1016/j.neuron.2018.08.022

Calhoun AJ, Tong A, Pokala N, Fitzpatrick JAJ, Sharpee TO, Chalasani SH. 2015. Neural mechanisms for evaluating environmental variability in

caenorhabditis elegans. *Neuron* **86**:428–441. doi:10.1016/j.neuron.2015.03.026

Chalasani SH, Chronis N, Tsunozaki M, Gray JM, Ramot D, Goodman MB, Bargmann CI. 2007. Dissecting a circuit for olfactory behaviour in Caenorhabditis elegans. *Nature* **450**:63–70. doi:10.1038/nature06292

Chalasani SH, Kato S, Albrecht DR, Nakagawa T, Abbott LF, Bargmann CI. 2010. Neuropeptide feedback modifies odor-evoked dynamics in Caenorhabditis elegans olfactory neurons. *Nat Neurosci* **13**:615–621. doi:10.1038/nn.2526

Chelur DS, Chalfie M. 2007. Targeted cell killing by reconstituted caspases. *Proc Natl Acad Sci U S A* **104**:2283–2288. doi:10.1073/pnas.0610877104

Cho SW, Choi KY, Park CS. 2004. A new putative cyclic nucleotide-gated channel gene, cng-3, is critical for thermotolerance in Caenorhabditis elegans. *Biochem Biophys Res Commun* **325**:525–531. doi:10.1016/j.bbrc.2004.10.060

Chou JH, Bargmann CI, Sengupta P. 2001. The Caenorhabditis elegans odr-2 gene encodes a novel Ly-6-related protein required for olfaction. *Genetics* **157**:211–224.

Chronis N, Zimmer M, Bargmann CI. 2007. Microfluidics for in vivo imaging of neuronal and behavioral activity in Caenorhabditis elegans. *Nat Methods* **4**:727–731. doi:10.1038/nmeth1075

Coburn CM, Bargmann CI. 1996. A putative cyclic nucleotide-gated channel is required for sensory development and function in C. elegans. *Neuron* **17**:695–706. doi:10.1016/S0896-6273(00)80201-9

Colosimo ME, Brown A, Mukhopadhyay S, Gabel C, Lanjuin AE, Samuel ADT, Sengupta P. 2004. Identification of Thermosensory and Olfactory Neuron-Specific Genes via Expression Profiling of Single Neuron Types. *Curr Biol* **14**:2245–2251. doi:10.1016/j.cub.2004.12.030

Daniels SA, Ailion M, Thomas JH, Sengupta P. 2000. egl-4 Acts through a transforming growth factor-β/SMAD pathway in Caenorhabditis elegans to regulate multiple neuronal circuits in response to sensory cues. *Genetics* **156**:123–141.

Drider D, Bekal S, Prévost H. 2004. Genetic organization and expression of citrate permease in lactic acid bacteria. *Genet Mol Res.* 3 (2): 273-281

Ferkey DM, Hyde R, Haspel G, Dionne HM, Hess HA, Suzuki H, Schafer WR, Koelle MR, Hart AC. 2007. C. elegans G Protein Regulator RGS-3 Controls

Sensitivity to Sensory Stimuli. *Neuron* **53**:39–52. doi:10.1016/j.neuron.2006.11.015

Fujiwara M, Aoyama I, Hino T, Teramoto T, Ishihara T. 2016. Gonadal Maturation Changes Chemotaxis Behavior and Neural Processing in the Olfactory Circuit of Caenorhabditis elegans. *Curr Biol* **26**:1522–1531. doi:10.1016/j.cub.2016.04.058

Fujiwara M, Sengupta P, McIntire SL. 2002. Regulation of body size and behavioral state of C. elegans by sensory perception and the egl-4 cGMP-dependent protein kinase. *Neuron* **36**:1091–1102. doi:10.1016/S0896-6273(02)01093-0

Gordus A, Pokala N, Levy S, Flavell SW, Bargmann CI. 2015. Feedback from network states generates variability in a probabilistic olfactory circuit. *Cell* **161**:215–227. doi:10.1016/j.cell.2015.02.018

Gray JM, Hill JJ, Bargmann CI. 2005. A circuit for navigation in Caenorhabditis elegans. *Proc Natl Acad Sci U S A* **102**:3184–3191. doi:10.1073/pnas.0409009101

Guillermin ML, Carrillo MA, Hallem EA. 2017. A Single Set of Interneurons Drives Opposite Behaviors in C. elegans. *Curr Biol* **27**:2630-2639.e6.

doi:10.1016/j.cub.2017.07.023

Hawk JD, Calvo AC, Liu P, Almoril-Porras A, Aljobeh A, Torruella-Suárez ML, Ren I, Cook N, Greenwood J, Luo L, Wang ZW, Samuel ADT, Colón-Ramos DA. 2018. Integration of Plasticity Mechanisms within a Single Sensory Neuron of C. elegans Actuates a Memory. *Neuron* **97**:356-367.e4. doi:10.1016/j.neuron.2017.12.027

Hobert O, Mori I, Yamashita Y, Honda H, Ohshima Y, Liu Y, Ruvkun G. 1997. Regulation of interneuron function in the C. elegans thermoregulatory pathway by the ttx-3 LIM homeobox gene. *Neuron* **19**:345–357. doi:10.1016/S0896-6273(00)80944-7

Itskovits E, Ruach R, Zaslaver A. 2018. Concerted pulsatile and graded neural dynamics enables efficient chemotaxis in C. elegans. *Nat Commun* **9**. 2866. doi:10.1038/s41467-018-05151-2

Jin H, Fishman ZH, Ye M, Wang L, Zuker CS. 2021. Top-Down Control of Sweet and Bitter Taste in the Mammalian Brain. *Cell* **184**:257-271.e16. doi:10.1016/j.cell.2020.12.014

Juang BT, Gu C, Starnes L, Palladino F, Goga A, Kennedy S, L'Etoile ND. 2013. Endogenous nuclear RNAi mediates behavioral adaptation to odor. *Cell*

154:1010–1022. doi:10.1016/j.cell.2013.08.006

Kim K, Colosimo ME, Yeung H, Sengupta P. 2005. The UNC-3 Olf/EBF protein represses alternate neuronal programs to specify chemosensory neuron identity. *Dev Biol* **286**:136–148. doi:10.1016/j.ydbio.2005.07.024

Kocabas A, Shen CH, Guo Z V., Ramanathan S. 2012. Controlling interneuron activity in Caenorhabditis elegans to evoke chemotactic behaviour. *Nature* **490**:273–277. doi:10.1038/nature11431

Koga M, Ohshima Y. 2004. The C. elegans ceh-36 Gene Encodes a Putative Homemodomain Transcription Factor Involved in Chemosensory Functions of ASE and AWC Neurons. *J Mol Biol* **336**:579–587. doi:10.1016/j.jmb.2003.12.037

Komatsu H, Mori I, Rhee JS, Akaike N, Ohshima Y. 1996. Mutations in a cyclic nucleotide-gated channel lead to abnormal thermosensation and chemosensation in C. elegans. *Neuron* **17**:707–718. doi:10.1016/S0896-6273(00)80202-0

Krzyzanowski MC, Brueggemann C, Ezak MJ, Wood JF, Michaels KL, Jackson CA, Juang BT, Collins KD, Yu MC, L'Etoile ND, Ferkey DM. 2013. The C. elegans cGMP-Dependent Protein Kinase EGL-4 Regulates Nociceptive

Behavioral Sensitivity. *PLoS Genet* **9**. doi:10.1371/journal.pgen.1003619

L'Etoile ND, Coburn CM, Eastham J, Kistler A, Gallegos G, Bargmann CI. 2002. The cyclic GMP-dependent protein kinase EGL-4 regulates olfactory adaptation in C. elegans. *Neuron* **36**:1079–1089. doi:10.1016/S0896-6273(02)01066-8

Lanjuin A, VanHoven MK, Bargmann CI, Thompson JK, Sengupta P. 2003. Otx/otd homeobox genes specify distinct sensory neuron identities in C. elegans. *Dev Cell* **5**:621–633. doi:10.1016/S1534-5807(03)00293-4

Larsch J, Flavell SW, Liu Q, Gordus A, Albrecht DR, Bargmann CI. 2015. A Circuit for Gradient Climbing in C. elegans Chemotaxis. *Cell Rep* **12**:1748–1760. doi:10.1016/j.celrep.2015.08.032

Larsch J, Ventimiglia D, Bargmann CI, Albrecht DR. 2013. High-throughput imaging of neuronal activity in Caenorhabditis elegans. *Proc Natl Acad Sci U S A* **110**. doi:10.1073/pnas.1318325110

Lee JI, O'Halloran DM, Eastham-Anderson J, Juang BT, Kaye JA, Hamilton OS, Lesch B, Goga A, L'Etoile ND. 2010. Nuclear entry of a cGMP-dependent kinase converts transient into long-lasting olfactory adaptation. *Proc Natl Acad Sci U S A* **107**:6016–6021. doi:10.1073/pnas.1000866107

Lesch BJ, Bargmann CI. 2010. The homeodomain protein hmbx-1 maintains asymmetric gene expression in adult C. elegans olfactory neurons. *Genes Dev* **24**:1802–1815. doi:10.1101/gad.1932610

Li Z, Liu J, Zheng M, Xu XZS. 2014. Encoding of both analog- and digital-like behavioral outputs by one C. Elegans interneuron. *Cell* **159**:751–765. doi:10.1016/j.cell.2014.09.056

Mok CA, Healey MP, Shekhar T, Leroux MR, Héon E, Zhen M. 2011. Mutations in a guanylate cyclase GCY-35/GCY-36 modify bardet-biedl syndrome-associated phenotypes in Caenorhabditis elegans. *PLoS Genet* **7**:31–32. doi:10.1371/journal.pgen.1002335

Nagai T, Yamada S, Tominaga T, Ichikawa M, Miyawaki A. 2004. Expanded dynamic range of fluorescent indicators for Ca2+ by circularly permuted yellow fluorescent proteins. *Proc Natl Acad Sci U S A* **101**:10554–10559. doi:10.1073/pnas.0400417101

Nakano S, Ikeda M, Tsukada Y, Fei X, Suzuki T, Niino Y, Ahluwalia R, Sano A, Kondo R, Ihara K, Miyawaki A, Hashimoto K, Higashiyama T, Mori I. 2020. Presynaptic MAST kinase controls opposing postsynaptic responses to convey stimulus valence in Caenorhabditis elegans. *Proc Natl Acad Sci U S*

A **117**:1638–1647. doi:10.1073/pnas.1909240117

O'Halloran DM, Altshuler-Keylin S, Zhang XD, He C, Morales-Phan C, Yu Y, Kaye JA, Brueggemann C, Chen TY, L'Etoile ND. 2017. Contribution of the cyclic nucleotide gated channel subunit, CNG-3, to olfactory plasticity in Caenorhabditis elegans. *Sci Rep* **7**:1–13. doi:10.1038/s41598-017-00126-7

Oda S, Tomioka M, Iino Y. 2011. Neuronal plasticity regulated by the insulin-like signaling pathway underlies salt chemotaxis learning in Caenorhabditis elegans. *J Neurophysiol* **106**:301–308. doi:10.1152/jn.01029.2010

Ohno H, Sakai N, Adachi T, Iino Y. 2017. Dynamics of Presynaptic Diacylglycerol in a Sensory Neuron Encode Differences between Past and Current Stimulus Intensity. *Cell Rep* **20**:2294–2303. doi:10.1016/j.celrep.2017.08.038

Ren P, Lim CS, Johnsen R, Albert PS, Pilgrim D, Riddle DL. 1996. Control of C. elegans larval development by neuronal expression of a TGF-β homolog. *Science (80-)* **274**:1389–1391. doi:10.1126/science.274.5291.1389

Roayaie K, Crump JG, Sagasti A, Bargmann CI. 1998. The Gα protein ODR-3 mediates olfactory and nociceptive function and controls cilium

morphogenesis in C. elegans olfactory neurons. *Neuron* **20**:55–67. doi:10.1016/S0896-6273(00)80434-1

Schackwitz WS, Inoue T, Thomas JH. 1996. Chemosensory neurons function in parallel to mediate a pheromone response in C. elegans. *Neuron* **17**:719–728. doi:10.1016/S0896-6273(00)80203-2

Sengupta P, Chou JH, Bargmann CI. 1996. odr-10 Encodes a seven transmembrane domain olfactory receptor required for responses to the odorant diacetyl. *Cell* **84**:899–909. doi:10.1016/S0092-8674(00)81068-5

Sengupta P, Colbert HA, Bargmann CI. 1994. The C. elegans gene odr-7 encodes an olfactory-specific member of the nuclear receptor superfamily. *Cell* **79**:971–980. doi:10.1016/0092-8674(94)90028-0

Shinkai Y, Yamamoto Y, Fujiwara M, Tabata T, Murayama T, Hirotsu T, Ikeda DD, Tsunozaki M, Iino Y, Bargmann CI, Katsura I, Ishihara T. 2011. Behavioral choice between conflicting alternatives is regulated by a receptor guanylyl cyclase, GCY-28, and a receptor tyrosine kinase, SCD-2, in AIA interneurons of Caenorhabditis elegans. *J Neurosci* **31**:3007–3015. doi:10.1523/JNEUROSCI.4691-10.2011

Shioi G, Shoji M, Nakamura M, Ishihara T, Katsura I, Fujisawa H, Takagi S.

2001. Mutations affecting nerve attachment of Caenorhabditis elegans. *Genetics* April 1, 2001 vol. 157 no. 4 1611-1622

Stringham EG, Dixon DK, Jones D, Candido EPM. 1992. Temporal and spatial expression patterns of the small heat shock (hsp16) genes in transgenic Caenorhabditis elegans. *Mol Biol Cell* **3**:221–233. doi:10.1091/mbc.3.2.221

Trent C, Tsuing N, Horvitz HR. 1983. Egg-laying defective mutants of the nematode Caenorhabditis elegans. *Genetics* **104**:619–647.

Troemel ER, Sagasti A, Bargmann CI. 1999. Lateral signaling mediated by axon contact and calcium entry regulates asymmetric odorant receptor expression in C. elegans. *Cell* **99**:387–398. doi:10.1016/S0092-8674(00)81525-1

Tsalik EL, Hobert O. 2003. Functional mapping of neurons that control locomotory behavior in Caenorhabditis elegans. *J Neurobiol* **56**:178–197. doi:10.1002/neu.10245

Tsunozaki M, Chalasani SH, Bargmann CI. 2008. A Behavioral Switch: cGMP and PKC Signaling in Olfactory Neurons Reverses Odor Preference in C. elegans. *Neuron* **59**:959–971. doi:10.1016/j.neuron.2008.07.038

Van Der Linden AM, Wiener S, You NJ, Kim K, Avery L, Sengupta P. 2008. The EGL-4 PKG acts with KIN-29 salt-inducible kinase and protein kinase A to

regulate chemoreceptor gene expression and sensory behaviors in Caenorhabditis elegans. *Genetics* **180**:1475–1491. doi:10.1534/genetics.108.094771

Ventimiglia D, Bargmann CI. 2017. Diverse modes of synaptic signaling, regulation, and plasticity distinguish two classes of C. elegans glutamatergic neurons. *Elife* **6**:1–25. doi:10.7554/eLife.31234

White JG, Southgate E, Thomson JN BS. 1986. The Structure of the Nervous System of the Nematode Caenorhabditis elegans. *Philos Trans R Soc London* **314**:1–340. doi:10.1098/rstb.1986.0056

Yu S, Avery L, Baude E, Garbers DL. 1997. Guanylyl cyclase expression in specific sensory neurons: A new family of chemosensory receptors. *Proc Natl Acad Sci U S A* **94**:3384–3387. doi:10.1073/pnas.94.7.3384

Figure legends

Figure 1: Primary sensory responses of olfactory neurons are not reduced in the *egl-4* mutant

(A) Chemotaxis indices to diacetyl (10^{-3} to 10^{-5} dilutions) of wild type [n=6 (10^{-3}), 9 (10^{-4}), 9 (10^{-5})], *egl-4(ky185)* [n=6 (10^{-3}), 9 (10^{-4}), 9 (10^{-5})] and *egl-4(n478)* [n=5 (10^{-3}), 8 (10^{-4}), 9 (10^{-5})]. **(B)** Chemotaxis indices to isoamyl alcohol (10^{-3} to 10^{-5} dilutions) of wild type [n= 9 (10^{-3}), 9 (10^{-4}), 9 (10^{-5})] and *egl-4(ky185)* [n=9 (10^{-3}), 9 (10^{-4}), 8 (10^{-5})]. **(A, B)** Error bars indicate s.e.m. *p<0.05, **p<0.01, ***p<0.001, one-way ANOVA with Dunnett's post-test (A), t-test (B). **(C)** Left, YC3.60 YFP/CFP ratio changes ($R/R_{0(ON)}$) (means ± s.e.m.) in wild-type and *egl-4(ky185)* AWA neurons. 10^{-7} dilution of diacetyl was used as stimulus. Right, average YFP/CFP ratio changes ($R/R_{0(ON)}$) at addition of the indicated diacetyl dilution in wild type [n=15 (10^{-5}), 13 (10^{-6}), 15 (10^{-7}), 9 (10^{-8}), 14 (10^{-9})] and *egl-4(ky185)* [n=14 (10^{-5}), 9 (10^{-6}), 14 (10^{-7}), 6 (10^{-8}), 15 (10^{-9})]. **(D)** Left, YC3.60 YFP/CFP ratio changes ($R/R_{0(OFF)}$) (means ± s.e.m.) in wild-type and *egl-4(ky185)* AWC neurons. 10^{-7} dilution of diacetyl was used as stimulus. Right, average YFP/CFP changes ($R/R_{0(OFF)}$) at removal of the indicated diacetyl dilution in wild type [n=21 (10^{-5}), 19 (10^{-6}), 17 (10^{-7}), 16

(10^{-8})] and *egl-4(ky185)* [n=13 (10^{-5}), 10 (10^{-6}), 17 (10^{-7}), 15 (10^{-8})]. **(C, D)** Gray-shaded box indicates the time period during which diacetyl was applied. Black bars under the response curve (left) indicate the time period used to calculate the average YFP/CFP ratio changes. Error bars indicate s.e.m. *p<0.05, t-test.

Figure 2: AIY interneuron of the *egl-4* mutant suppresses chemotaxis to diacetyl but not to isoamyl alcohol

(A) Chemotaxis indices to diacetyl (10^{-3} and 10^{-4} dilutions) of *egl-4(ky185)* whose AIA interneuron was ablated by caspase expression. **(B)** Chemotaxis indices to diacetyl (10^{-4} dilution) of e*gl-4(ky185)* whose AIB interneuron was ablated by caspase expression. **(C)** Chemotaxis indices to diacetyl (10^{-2}, 1/2000 and 10^{-4} dilution) of e*gl-4(ky185)* whose AIY interneuron was ablated by caspase expression. **(D)** Chemotaxis indices to isoamyl alcohol (10^{-3} and 10^{-4} dilution) of e*gl-4(ky185)* whose AIY interneuron was ablated by caspase expression. **(A-D)** Error bars indicate s.e.m. *p<0.05, **p<0.01, two-way ANOVA with Tukey's post-test. The number of assayed plates is indicated for each data point.

Figure 3: AIY in the *egl-4* mutant shows reversed Ca^{2+} response to diacetyl stimuli, but not to isoamyl alcohol

(A, B) Left, YC2.60 YFP/CFP ratio changes ($R/R_{0(ON)}$) (mean ± s.e.m.) in wild-type and *egl-4(ky185)* AIY interneurons in response to 10^{-7} diacetyl (A) and 10^{-4} isoamyl alcohol (B). Shaded box indicates the time period during which the indicated odorant was applied. Black bars under the response curve indicate the time period used to calculate the average YFP/CFP ratio changes. Right, average YFP/CFP ratio changes at odorant addition (22–27 sec) (a) and at odorant removal (80–90 sec) (b). To calculate average YFP/CFP ratio changes, YFP/CFP ratio were normalized by the preceding 5-sec period of odor addition (15–20 sec, $R_{0(ON)}$) for (a), or of odor removal (75–80 sec, $R_{0(OFF)}$) for (b). Error bars indicate s.e.m. ***$p<0.001$, t-test. The number of tested worms is indicated in parentheses.

Figure 4: Enhanced AWC response does not reverse the AIY response

(A) Left, YC3.60 YFP/CFP ratio changes ($R/R_{0(OFF)}$) (mean ± s.e.m.) in wild-type AWC neurons in response to removal of 10^{-5} diacetyl after 1 or 5 min exposure. The time period of 30-sec before and 30-sec after odor removal is

shown. Shaded box indicates the time period during which diacetyl was applied. Black bars under the response curve indicate the time period used to calculate the average YFP/CFP ratio changes. Right, average YFP/CFP ratio changes ($R/R_{0(OFF)}$) in the 10-sec period immediately after diacetyl removal. Error bars indicate s.e.m. ***p<0.001, t-test. Sample numbers are indicated in parentheses. **(B)** Left, YC2.60 YFP/CFP ratio changes ($R/R_{0(ON)}$) (mean ± s.e.m.) in wild type AIY neurons in response to 1 or 5 min exposure to 10^{-5} diacetyl. Shaded box indicates the time period during which diacetyl was applied. Black bars under the response curve indicate the time period used to calculate the average YFP/CFP ratio changes. Right, average YFP/CFP ratio changes ($R/R_{0(OFF)}$) in the 10-sec period immediately after diacetyl removal. To calculate average YFP/CFP ratio changes ($R/R_{0(OFF)}$), YFP/CFP ratio were normalized to the average YFP/CFP ratio of the preceding 5-sec period of odor removal. Error bars indicate s.e.m. n.s. p>0.05, t-test. The number of tested worms is indicated in parentheses.

Figure 5: Both AWA and AWC olfactory neurons are required for the reversed AIY response of the *egl-4* mutant

(A–C) Left, YC2.60 YFP/CFP ratio changes ($R/R_{0(ON)}$) (mean ± s.e.m.) in AIY interneurons in response to diacetyl (10^{-7} dilution) in wild type and *egl-4(ky185)* (A), *ceh-36(ks86)* and *egl-4(ky185); ceh-36(ks86)* (B), *odr-7(ky4)* and *egl-4(ky185); odr-7(ky4)* (C). Shaded box indicates the time period during which the indicated odorant was applied. Black bars under the response curve indicate the time period used to calculate the average YFP/CFP ratio changes. Right, average YFP/CFP ratio changes at odorant addition (22–27 sec) (a) and at odorant removal (80–90 sec) (b). To calculate average YFP/CFP ratio changes, YFP/CFP ratio were normalized by the preceding 5-sec period of odor addition (15–20 sec, $R_{0(ON)}$) for (a), or of odor removal (75–80 sec, $R_{0(OFF)}$) for (b). Error bars indicate s.e.m.**$p<0.01$, two-way ANOVA with Tukey's post-test. The number of tested worms is indicated in parentheses.

Figure 6: EGL-4 acts in AWA and ASI sensory neurons to prevent AIY from eliciting the reversed response and to promote chemotaxis

(A, B) The cell-specific expression of an *egl-4* cDNA driven by various promoters was tested for rescue activity of defective chemotaxis to diacetyl of the *egl-4* mutant. Each transgene was introduced into the *egl-4(ky185)* mutant as an

extrachromosomal array. Control animals (Ex-) and animals with a transgene (Ex+) were compared. Ex- and Ex+ animals were cultured on the same culture plate and tested on the same assay plate. For each genotype except H20p strain, 2-3 transgenic lines were examined, and they showed same phenotype. Data of representative lines are shown. Error bars indicate s.e.m. *$p<0.05$, t-test. The number of assay plates is indicated for each data point. (C) The cellular expression patterns driven by each promoter are shown. (D) In the *egl-4(ky185)* background, *egl-4* cDNA was expressed in AWA solely (by *odr-10p*) or in both AWA and ASI (by *gpa-4p*), and Ca^{2+} responses of AIY were examined. Left, YC2.60 YFP/CFP ratio changes ($R/R_{0(ON)}$) (means ± s.e.m.) to diacetyl (10^{-7} dilution) in AIY interneuron of wild type and *egl-4(ky185)* expressing the transgene. Gray-shaded box indicates the time period during which diacetyl was applied. Black bars under the response curve indicate the time period used to calculate the average YFP/CFP ratio changes. The number of tested worms is indicated in parentheses. Right, average YFP/CFP ratio changes at 22–27 sec (a) and at 80–90 sec (b). To calculate average YFP/CFP ratio changes, YFP/CFP ratio were normalized by the preceding 5-sec period of odor addition (15–20 sec, $R_{0(ON)}$) for (a), or of odor removal (75–80 sec, $R_{0(OFF)}$) for (b). Error bars

indicate s.e.m. *p<0.05, **p<0.01, two-way ANOVA with Dunnett's post-test. **(E)** The expression of an *egl-4* cDNA was induced in the *egl-4(ky185)* mutant by heat shock in the adult stage, and chemotaxis to diacetyl (10^{-4} dilution) was tested. The transgene was introduced into the *egl-4(ky185)* mutant as an extrachromosomal array. Control animals (Ex-) and animals with a transgene (Ex+) were compared. Ex- and Ex+ animals were cultured on the same culture plate and tested on the same assay plate. Error bars indicate s.e.m. **p<0.01, two-way ANOVA with Tukey's post-test. The number of assay plates is indicated for each data point.

Figure 7: AIB in the *egl-4* mutant shows decreased Ca^{2+} response to diacetyl stimuli

Left, YC3.60 YFP/CFP ratio changes ($R/R_{0(ON)}$) (mean ± s.e.m.) in wild-type and *egl-4(ky185)* AIB interneurons in response to 10^{-7} diacetyl. Shaded box indicates the time period during which diacetyl was applied. Right, average YFP/CFP ratio changes during diacetyl application (30–90 sec). To calculate average YFP/CFP ratio changes, YFP/CFP ratio were normalized by the preceding 30-sec period of odor addition (0–30 sec, $R_{0(ON)}$). Error bars indicate

s.e.m. ***p<0.001, t-test. The number of tested worms is indicated in parentheses.

Supplementary Figure 1: The *egl-4* mutation does not affect the expression level of ODR-10

(A) Representative image of ODR-10-tagged GFP fluorescence in the head region of a wild-type animal. Left, differential interference contrast image. Right, fluorescence image. White arrow indicates fluorescence of ODR-10-tagged GFP. **(B)** The percentages of animals with indicated fluorescence levels of ODR-10-tagged GFP in wild type and *egl-4(ky185)*. Sample numbers are indicated in parentheses. Scale bar = 10 μm.

Supplementary Figure 2: Chemotaxis of the *egl-4* mutant which lacks AIY by *ttx-3* mutation

(A) Chemotaxis indices to diacetyl (10^{-2} to 10^{-4} dilutions) of wild type (n=9), *egl-4(ky185)* (n=8–9), *ttx-3(ks5)* (n=6–9) and *egl-4(ky185); ttx-3(ks5)* (n=9). Error bars indicate s.e.m. *p<0.05, ***p<0.001, two-way ANOVA with Tukey's post-test. **(B)** A *ttx-3* cDNA was expressed specifically in AIY in the

egl-4(ky185); ttx-3(ks5) double mutant and the animals were tested for chemotaxis to diacetyl (1/2000 dilution) {WT, n=15; *ttx-3(ks5)*, n=9; *egl-4(ky185)*, n=14; *egl-4(ky185); ttx-3(ks5)*, n=14; *egl-4(ky185); ttx-3(ks5); Ex[AIYp::ttx-3]*, n=14}. Error bars indicate s.e.m. *p<0.05, **p<0.01, two-way ANOVA with Dunnett's post-test.

Supplementary Figure 3: AIY Ca^{2+} response to 10^{-5} diacetyl in the *egl-4* mutant

(A) Left, YC2.60 YFP/CFP ratio changes (mean ± s.e.m.) in wild type and *egl-4(ky185)* AIY interneuron in response to 10^{-5} diacetyl. Shaded box indicates the time period during which diacetyl was applied. Black bars under the response curve indicate the time period used to calculate the average YFP/CFP ratio changes. Right, average YFP/CFP ratio changes at 22–27 sec (a) and 80–90 sec (b) indicated in the left panel. To calculate average YFP/CFP ratio changes, YFP/CFP ratio changes of each recording were normalized to the average YFP/CFP ratio of the preceding 5-sec period [15–20 sec for (a) and 75–80 sec for (b)]. Error bars indicate s.e.m. **p<0.01, ***p<0.001, t-test. Sample numbers are indicated in parentheses.

Supplementary Figure 4: AIY Ca^{2+} response of the *egl-4* mutant whose AWC was ablated by caspase expression

We confirmed AIY Ca^{2+} responses in the absence of AWC by using strains in which AWC was ablated by caspase expression. For the purpose, we utilized the wild type animals and the *egl-4* mutant harboring *Is[odr-1::mCasp1.mec-4::gfp]* that is a transgene which directs the ablation of AWC and AWB neurons. Although the Ca^{2+} responses to the odorant were fluctuated, AIY in the *egl-4* mutant lacking AWC and AWB did not exhibit neither the Ca^{2+} decrease at diacetyl addition nor the significant Ca^{2+} increase at diacetyl removal, being different from the *egl-4* mutant. Left, YC2.60 YFP/CFP ratio changes (mean ± s.e.m.) in AIY interneuron in response to diacetyl (10^{-7} dilution) in AWB and AWC ablated *egl-4(ky185)* animals. Shaded box indicates the time period during which the indicated odorant was applied. Black bars under the response curve indicate the time period used to calculate the average YFP/CFP ratio changes. Right, average YFP/CFP ratio changes at 22–27 sec (a) and 80–90 sec (b). The data of wild type and the *egl-4* mutant are same as in Figure 3A, and are shown here for comparison. To calculate average YFP/CFP ratio changes, YFP/CFP ratio changes of each recording were normalized to the average YFP/CFP ratio

of the preceding 5-sec period [15–20 sec for (a) and 75–80 sec for (b)]. Error bars indicate s.e.m. n.s. $p>0.05$, two-way ANOVA with Tukey's post-test. Sample numbers are indicated in parentheses.

Supplementary Table 1: Analyses of the AIY response upon odor stimulation

The Sizes of AIY Ca^{2+} change at odor addition and removal were statistically analyzed in each genotype. Colored areas indicate the changes we described in the manuscript as "increase of Ca^{2+}" or "decrease of Ca^{2+}". Red letters indicate $p<0.05$. The average YFP/CFP ratio during pre- and post-timeframe of odor addition (for ON response) as well as pre- and post-timeframe of odor removal (for OFF response) are shown. To examine if odor addition and odor removal induced significant changes in the YFP/CFP ratio, we compared the average YFP/CFP ratio of the pre- and post-timeframe by paired two-tailed t-test. For analyses, we used 5-sec or 10-sec timeframe. We could capture rapid changes by using 5-sec timeframe and slower changes by using 10-sec timeframe. Pre-timeframes are set just before odor addition and removal, and post-timeframes are set 2 sec after odor addition and removal (see Table S1). Since AIY response of *egl-4; odr-7* animals to diacetyl addition was slow and gradual, we also analyzed 10-sec post-timeframe that was shifted to 10 sec after odor addition, and compared that with

10-sec pre-timeframe that was set just before odor addition (* in Table S1).

We noticed that the YFP/CFP ratio in strains with the *egl-4* mutation was generally higher than the ratio in the other strains. However, *egl-4* expression in both AWA and ASI, which restored the normal AIY OFF response in the *egl-4* mutant, did not change the YFP/CFP ratio. Thus, we concluded that the high YFP/CFP ratio does not directly reflect the EGL-4 function for regulating AIY response properties, and did not pursue further here.

Supplementary Table 2: *C. elegans* strains and transgenic lines used in this study

Figure 1

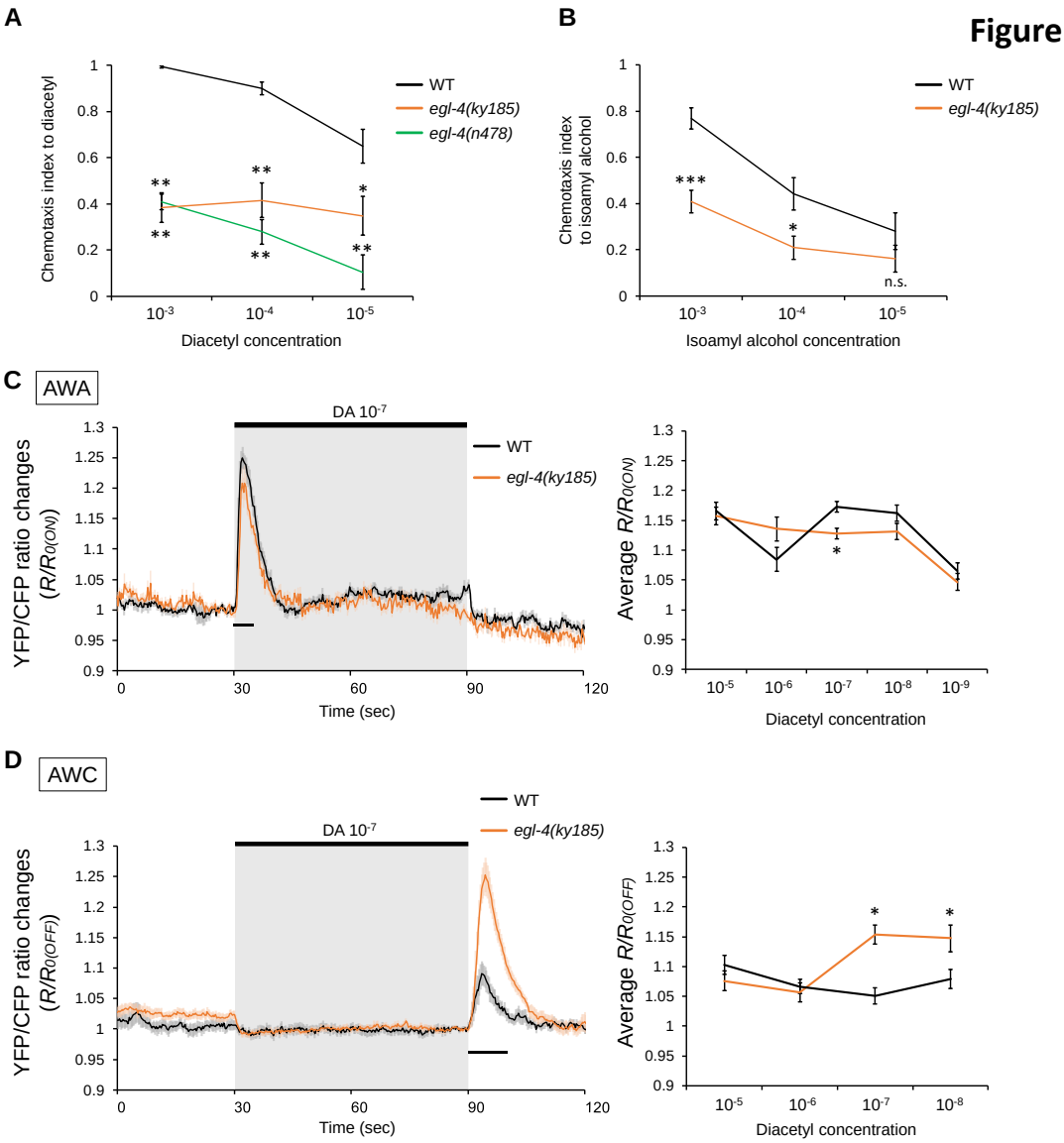
A
Chemotaxis index to diacetyl
WT
egl-4(ky185)
egl-4(n478)
Diacetyl concentration
B
Chemotaxis index to isoamyl alcohol
WT
egl-4(ky185)
n.s.
Isoamyl alcohol concentration
C
AWA
DA 10-7
YFP/CFP ratio changes (R/R0(ON))
WT
egl-4(ky185)
Time (sec)
Average R/R0(ON)
Diacetyl concentration
D
AWC
DA 10-7
YFP/CFP ratio changes (R/R0(OFF))
WT
egl-4(ky185)
Time (sec)
Average R/R0(OFF)
Diacetyl concentration

Figure 2

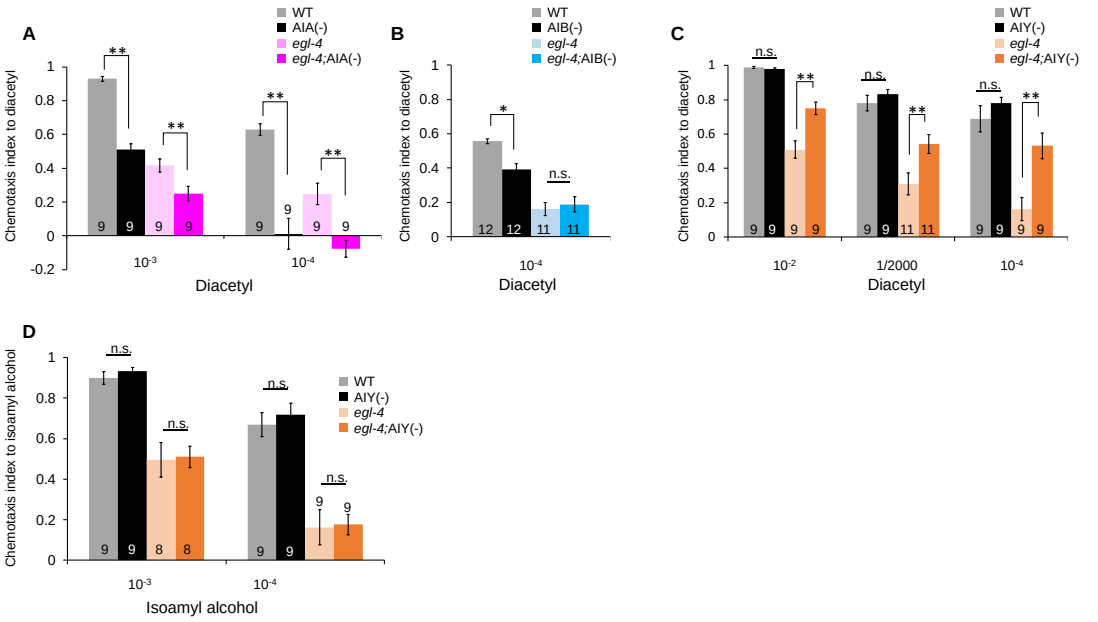
A
WT
AIA(-)
egl-4
egl-4;AIA(-)
Chemotaxis index to diacetyl
Diacetyl
B
WT
AIB(-)
egl-4
egl-4;AIB(-)
Chemotaxis index to diacetyl
Diacetyl
C
WT
AIY(-)
egl-4
egl-4;AIY(-)
Chemotaxis index to diacetyl
Diacetyl
D
WT
AIY(-)
egl-4
egl-4;AIY(-)
Chemotaxis index to isoamyl alcohol
Isoamyl alcohol

Figure 3

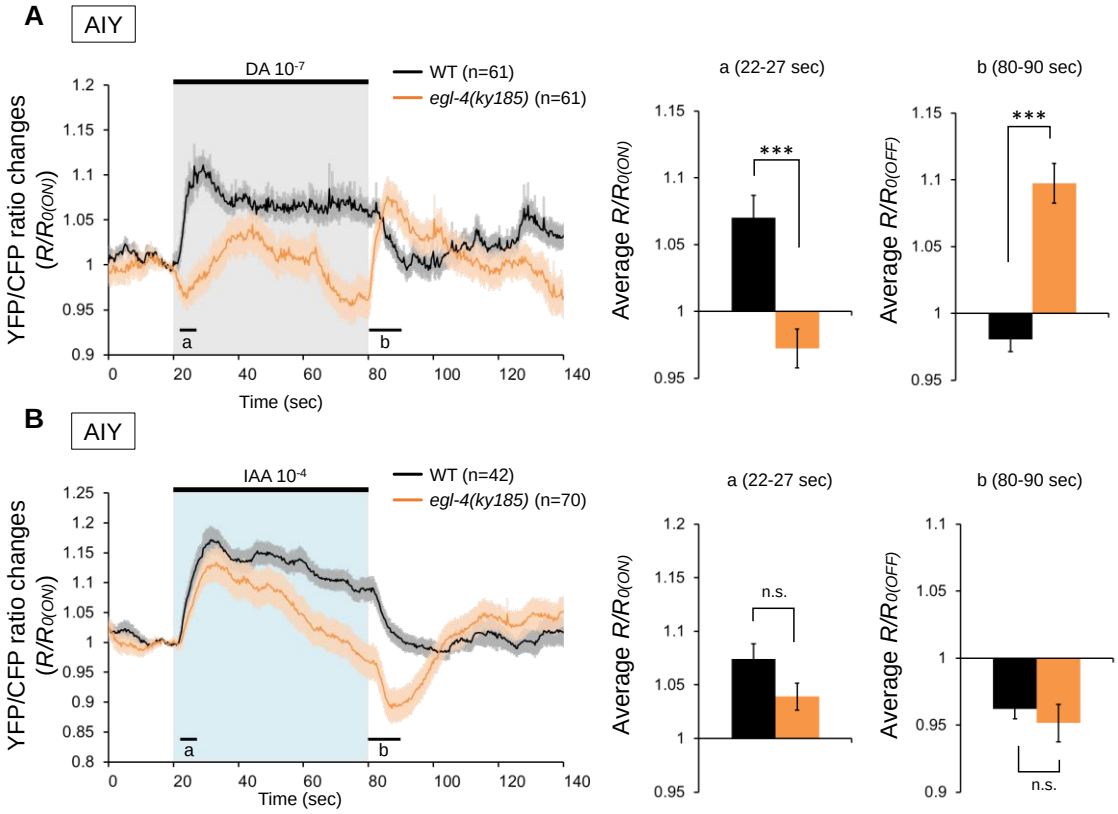
A
AIY
DA 10-7
WT (n=61)
egl-4(ky185) (n=61)
YFP/CFP ratio changes (R/R0(ON))
Time (sec)
a
b
a (22-27 sec)
b (80-90 sec)
Average R/R0(ON)
Average R/R0(OFF)
***
B
AIY
IAA 10-4
WT (n=42)
egl-4(ky185) (n=70)
n.s.

Figure 4

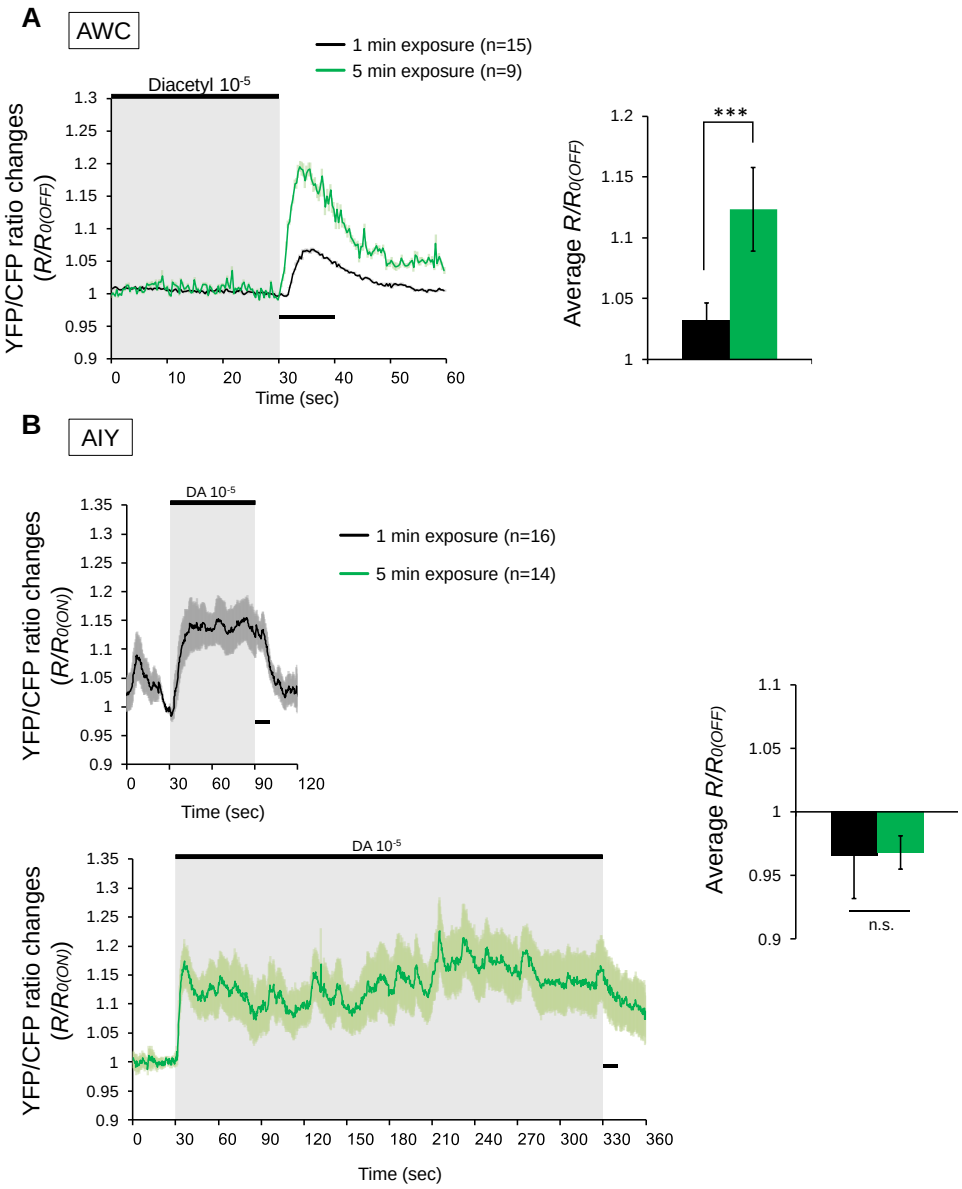
A
AWC
1 min exposure (n=15)
5 min exposure (n=9)
Diacetyl 10-5
YFP/CFP ratio changes (R/R0(OFF))
Time (sec)
Average R/R0(OFF)
***
B
AIY
DA 10-5
1 min exposure (n=16)
5 min exposure (n=14)
YFP/CFP ratio changes (R/R0(ON))
Time (sec)
Average R/R0(OFF)
n.s.

Figure 5

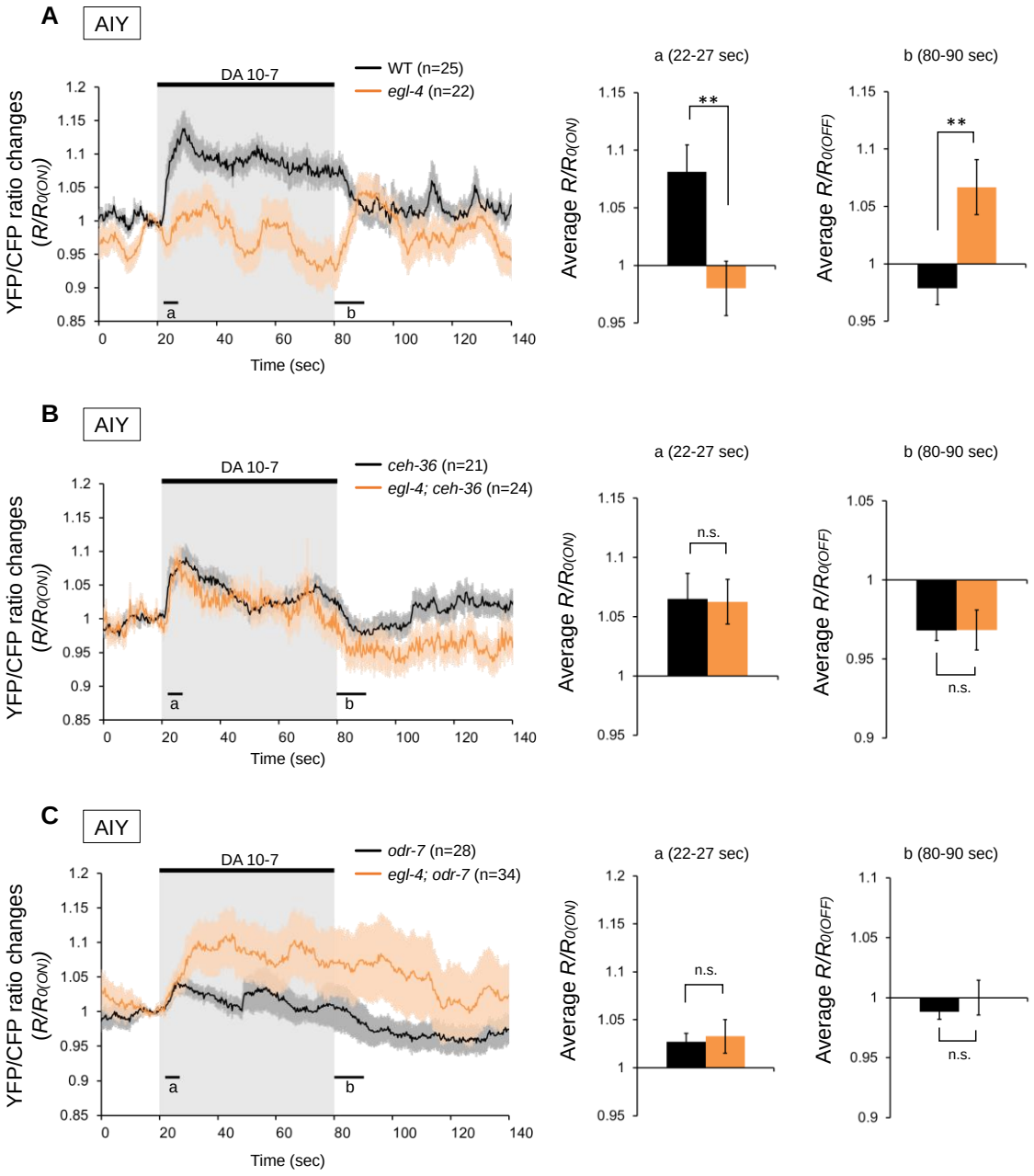
A
AIY
DA 10-7
WT (n=25)
egl-4 (n=22)
YFP/CFP ratio changes (R/R0(ON))
Time (sec)
a (22-27 sec)
b (80-90 sec)
Average R/R0(ON)
Average R/R0(OFF)
**
B
AIY
DA 10-7
ceh-36 (n=21)
egl-4; ceh-36 (n=24)
n.s.
C
AIY
DA 10-7
odr-7 (n=28)
egl-4; odr-7 (n=34)
n.s.

Figure 6

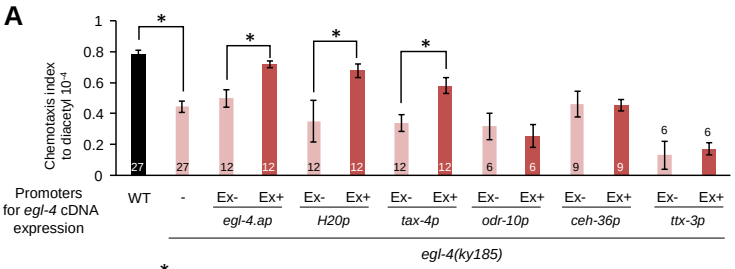

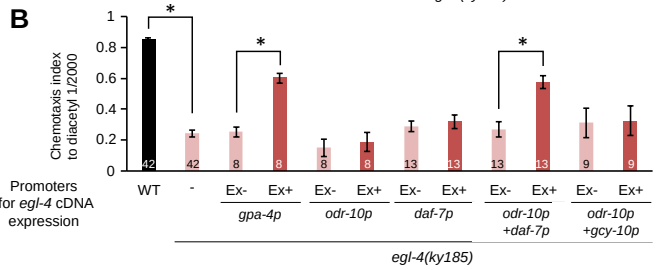

C

Promoter	Cellular patterns of expression
H20p	All neurons
tax-4p	AWB AWC ASE AFD ASI ASJ ASK ASG URX BAG
ceh-36p	AWC ASE
ttx-3p	AIY
odr-10p	AWA
gpa-4p	AWA ASI
daf-7p	ASI
gcy-10p	AWB AWC

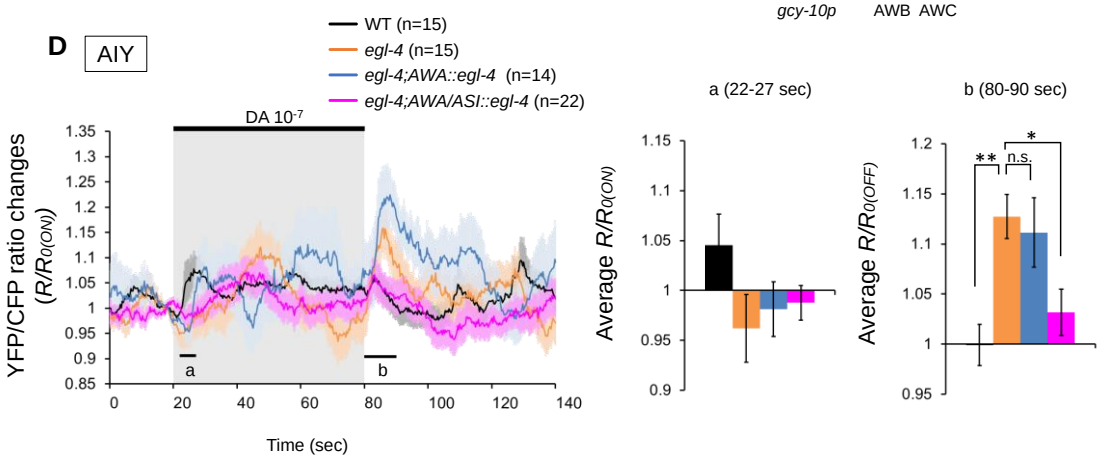

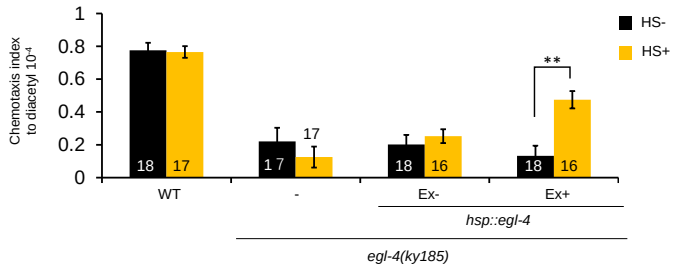

Figure 7

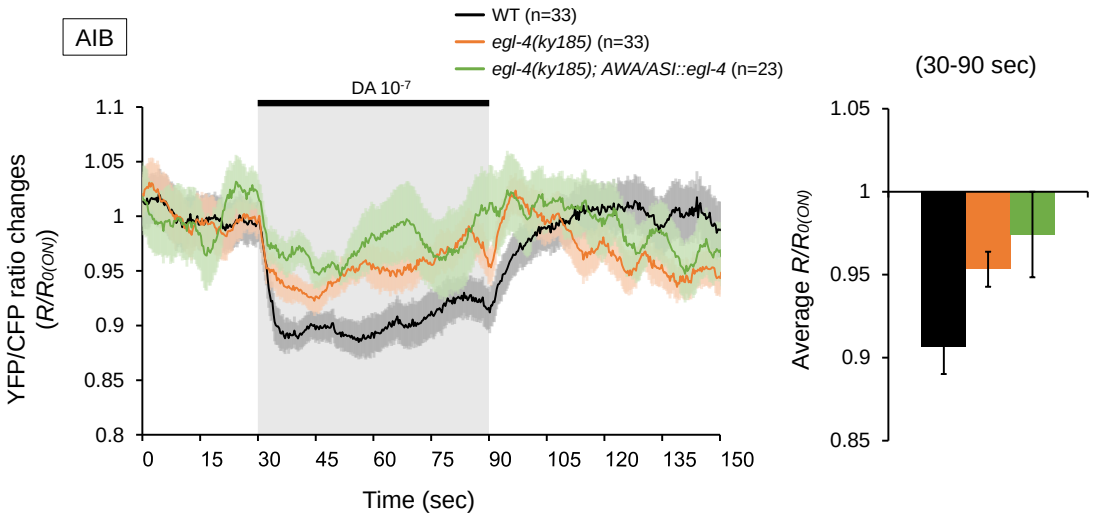
AIB
WT (n=33)
egl-4(ky185) (n=33)
egl-4(ky185); AWA/ASI::egl-4 (n=23)
DA 10-7
YFP/CFP ratio changes
(R/R0(ON))
1.1
1.05
1
0.95
0.9
0.85
0.8
0
15
30
45
60
75
90
105
120
135
150
Time (sec)
(30-90 sec)
Average R/R0(ON)
1.05
1
0.95
0.9
0.85

A

Expression of ODR-10 tagged GFP in wild type

Figure S1

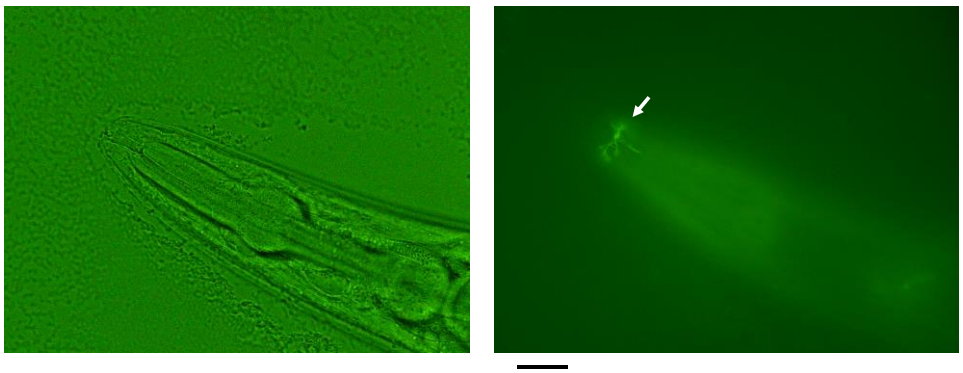

B

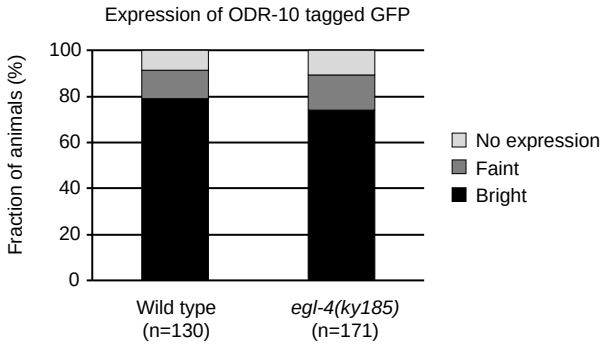

Figure S2

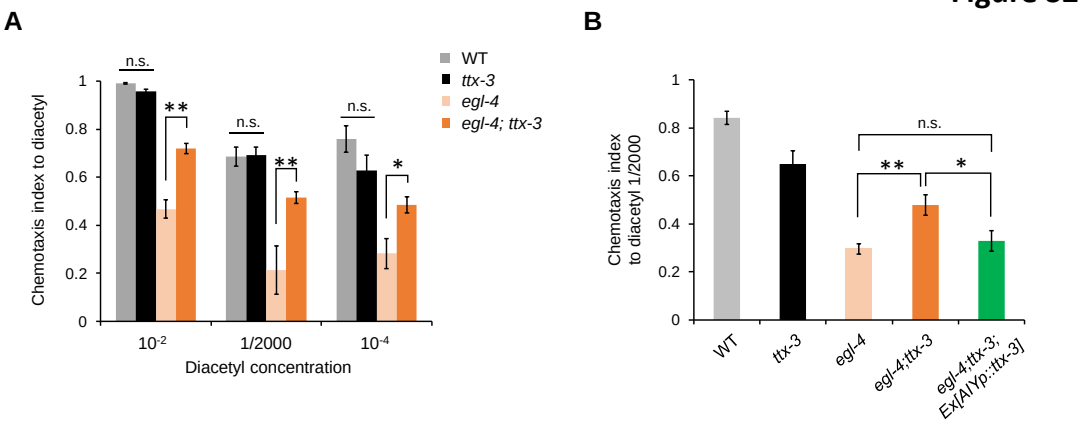
A
B
WT
ttx-3
egl-4
egl-4; ttx-3
Chemotaxis index to diacetyl
n.s.
**
*
1
0.8
0.6
0.4
0.2
0
10-2
1/2000
10-4
Diacetyl concentration
Chemotaxis index to diacetyl 1/2000
WT
ttx-3
egl-4
egl-4;ttx-3
egl-4;ttx-3; Ex[AIYp::ttx-3]

Figure S3

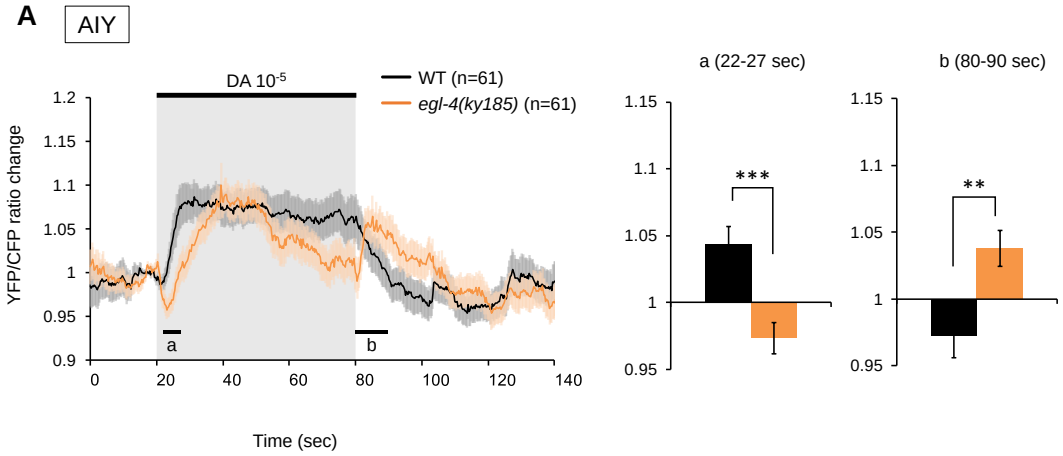
A
AIY
DA 10-5
WT (n=61)
egl-4(ky185) (n=61)
YFP/CFP ratio change
Time (sec)
a
b
a (22-27 sec)
b (80-90 sec)
***
**

Figure S4

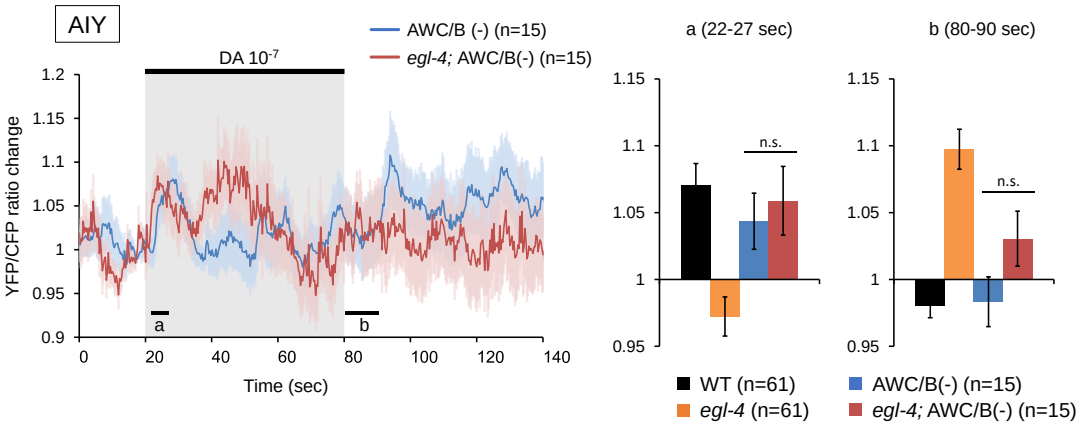
AIY
AWC/B (-) (n=15)
egl-4; AWC/B(-) (n=15)
DA 10-7
YFP/CFP ratio change
Time (sec)
a
b
a (22-27 sec)
b (80-90 sec)
n.s.
n.s.
WT (n=61)
egl-4 (n=61)
AWC/B(-) (n=15)
egl-4; AWC/B(-) (n=15)

Figure S5

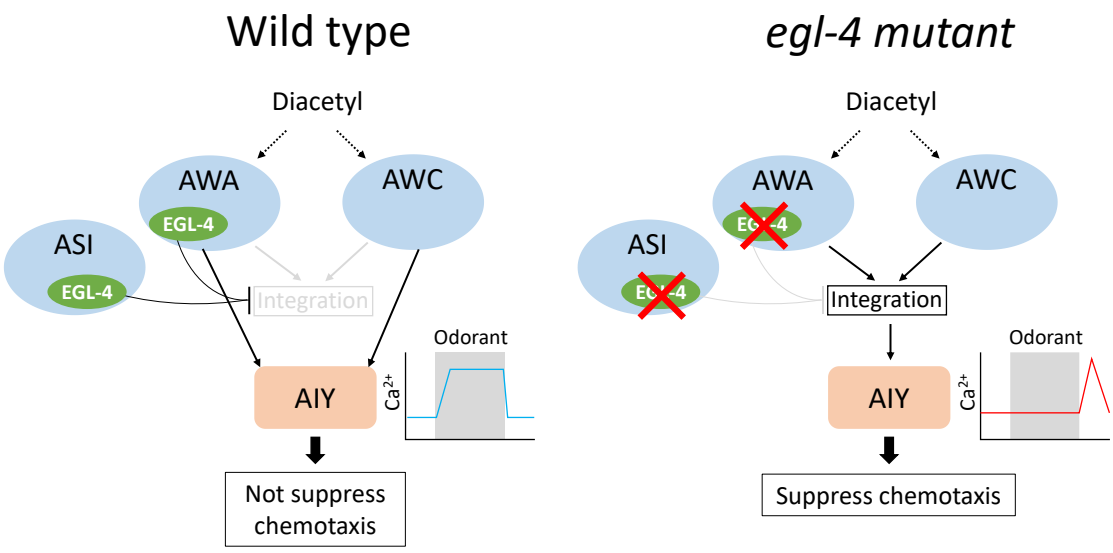
Wild type
Diacetyl
AWA
EGL-4
AWC
ASI
EGL-4
Integration
Odorant
AIY
Ca2+
Not suppress chemotaxis
egl-4 mutant
Diacetyl
AWA
AWC
ASI
Integration
Odorant
AIY
Ca2+
Suppress chemotaxis

Figure S6

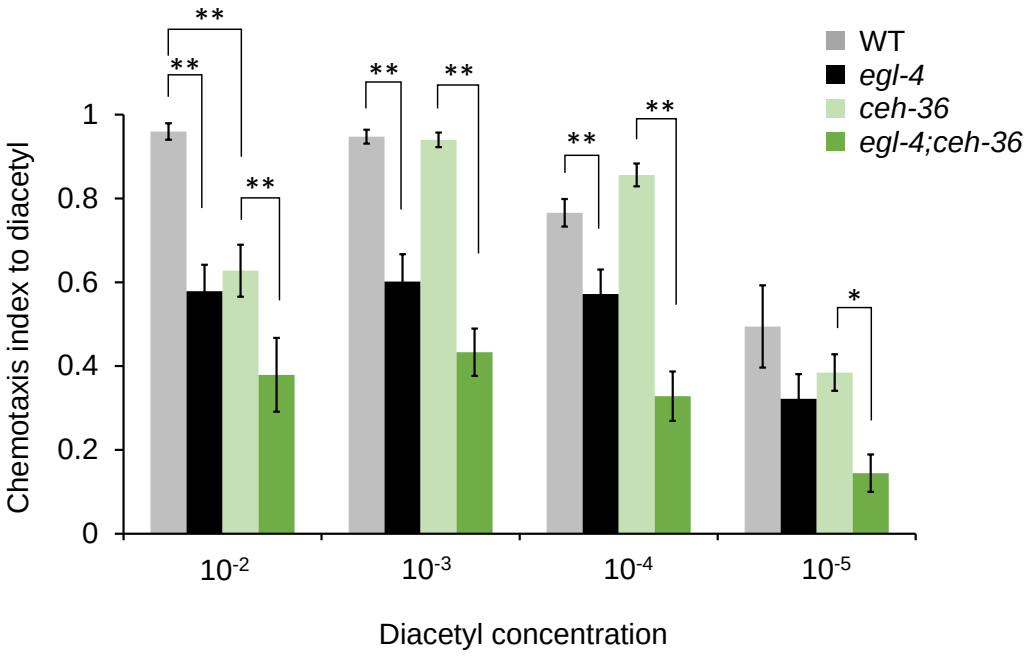
WT
egl-4
ceh-36
egl-4;ceh-36
Chemotaxis index to diacetyl
0
0.2
0.4
0.6
0.8
1
**
**
**
**
**
**
**
**
*
10-2
10-3
10-4
10-5
Diacetyl concentration

Table S1

Odor	Strain	n		Time window		Average	s.e.m.	Difference (post-pre)	p-value
DA10-7	N2 (Figure 3A)	61	ON response	10-sec period	pre (10-20s)	3.85	0.097		
					post (22-32s)	4.14	0.100	0.289	1.6E-05
				5-sec period	pre (15-20s)	3.84	0.095		
					post (22-27s)	4.08	0.101	0.246	0.0006
			OFF response	10-sec period	pre (70-80s)	4.08	0.107		
					post (82-92s)	3.92	0.091	-0.158	0.0015
				5-sec period	pre (75-80s)	4.06	0.105		
					post (82-87s)	3.99	0.097	-0.076	0.0684
	egl-4(ky185)	61	ON response	10-sec period	pre (10-20s)	7.59	0.278		
	(Figure 3A)				post (22-32s)	7.41	0.286	-0.177	0.1448
				5-sec period	pre (15-20s)	7.58	0.276		
					post (22-27s)	7.35	0.284	-0.227	0.0334
			OFF response	10-sec period	pre (70-80s)	7.24	0.286		
					post (82-92s)	7.88	0.246	0.637	4.0E-07
				5-sec period	pre (75-80s)	7.23	0.287		
					post (82-87s)	7.87	0.257	0.631	6.4E-07
	ceh-36(ks86)	21	ON response	10-sec period	pre (10-20s)	3.90	0.086		
	(Figure 5B)				post (22-32s)	4.18	0.137	0.277	0.0054
				5-sec period	pre (15-20s)	3.89	0.086		
					post (22-27s)	4.15	0.142	0.262	0.0089
			OFF response	10-sec period	pre (70-80s)	4.01	0.101		
					post (82-92s)	3.83	0.094	-0.185	9.4E-05
				5-sec period	pre (75-80s)	3.99	0.102		
					post (82-87s)	3.85	0.094	-0.136	4.9E-05
	egl-4(ky185);	24	ON response	10-sec period	pre (10-20s)	7.27	0.373		
	ceh-36(ks86)				post (22-32s)	7.60	0.353	0.338	0.0025
	(Figure 5B)			5-sec period	pre (15-20s)	7.22	0.363		
					post (22-27s)	7.61	0.345	0.396	0.0046
			OFF response	10-sec period	pre (70-80s)	7.24	0.375		
					post (82-92s)	6.87	0.364	-0.361	0.0009
				5-sec period	pre (75-80s)	7.15	0.380		
					post (82-87s)	6.90	0.378	-0.258	0.0142
	odr-7(ky4)	28	ON response	10-sec period	pre (10-20s)	3.74	0.118		
	(Figure 5C)				post (22-32s)	3.83	0.116	0.096	0.0523
				5-sec period	pre (15-20s)	3.74	0.117		
					post (22-27s)	3.82	0.119	0.073	0.0497
			OFF response	10-sec period	pre (70-80s)	3.77	0.127		
					post (82-92s)	3.72	0.141	-0.049	0.1782
				5-sec period	pre (75-80s)	3.78	0.141		
					post (82-87s)	3.75	0.147	-0.033	0.1815
	egl-4(ky185);	34	ON response	10-sec period	pre (10-20s)	5.96	0.334		
	odr-7(ky4)				post (22-32s)	6.20	0.344	0.242	0.1270
	(Figure 5C)				post (30-40s)(*)	6.38	0.360	0.423	0.0442
				5-sec period	pre (15-20s)	5.94	0.331		
					post (22-27s)	6.10	0.340	0.160	0.1750
			OFF response	10-sec period	pre (70-80s)	6.17	0.321		
					post (82-92s)	6.02	0.265	-0.156	0.2476
				5-sec period	pre (75-80s)	6.12	0.313		
					post (82-87s)	6.02	0.271	-0.094	0.3839

Table S1

Odor	Strain	n		Time window		Average	s.e.m.	Difference (post-pre)	p-value
DA10-7	egl-4; Ex[AWA::egl-4] (Figure 6D)	14	ON response	10-sec period	pre (10-20s)	6.28	0.367		
					post (22-32s)	6.34	0.435	0.058	0.8076
				5-sec period	pre (15-20s)	6.19	0.374		
					post (22-27s)	6.12	0.458	-0.067	0.6879
			OFF response	10-sec period	pre (70-80s)	6.51	0.459		
					post (82-92s)	7.03	0.352	0.514	0.0718
				5-sec period	pre (75-80s)	6.43	0.390		
					post (82-87s)	6.95	0.408	0.516	0.0248
	egl-4; Ex[AWA/ASI::egl-4] (Figure 6D)	22	ON response	10-sec period	pre (10-20s)	8.52	0.598		
					post (22-32s)	8.46	0.554	-0.059	0.7777
				5-sec period	pre (15-20s)	8.56	0.591		
					post (22-27s)	8.44	0.570	-0.126	0.4588
			OFF response	10-sec period	pre (70-80s)	8.55	0.554		
					post (82-92s)	8.65	0.501	0.096	0.6354
				5-sec period	pre (75-80s)	8.55	0.546		
					post (82-87s)	8.73	0.498	0.180	0.3621
DA10-5	N2 (Figure 3B)	34	ON response	10-sec period	pre (10-20s)	3.69	0.107		
					post (22-32s)	3.90	0.113	0.209	0.0033
				5-sec period	pre (15-20s)	3.71	0.117		
					post (22-27s)	3.80	0.106	0.086	0.1619
			OFF response	10-sec period	pre (70-80s)	3.90	0.106		
					post (82-92s)	3.72	0.100	-0.180	0.0261
				5-sec period	pre (75-80s)	3.90	0.105		
					post (82-87s)	3.78	0.103	-0.117	0.1135
	egl-4(ky185) (Figure 3B)	82	ON response	10-sec period	pre (10-20s)	7.32	0.222		
					post (22-32s)	7.31	0.226	-0.011	0.9165
				5-sec period	pre (15-20s)	7.38	0.224		
					post (22-27s)	7.16	0.226	-0.224	0.0113
			OFF response	10-sec period	pre (70-80s)	7.42	0.250		
					post (82-92s)	7.60	0.216	0.180	0.1020
				5-sec period	pre (75-80s)	7.42	0.247		
					post (82-87s)	7.64	0.222	0.221	0.0251
IAA10-4	N2 (Figure S3)	42	ON response	10-sec period	pre (10-20s)	3.59	0.108		
					post (22-32s)	4.03	0.162	0.441	4.0E-07
				5-sec period	pre (15-20s)	3.59	0.105		
					post (22-27s)	3.87	0.147	0.285	5.1E-05
			OFF response	10-sec period	pre (70-80s)	3.91	0.119		
					post (82-92s)	3.66	0.098	-0.250	8.5E-07
				5-sec period	pre (75-80s)	3.89	0.119		
					post (82-87s)	3.74	0.106	-0.153	2.4E-05
	egl-4(ky185) (Figure S3)	70	ON response	10-sec period	pre (10-20s)	6.83	0.175		
					post (22-32s)	7.37	0.195	0.538	5.6E-06
				5-sec period	pre (15-20s)	6.87	0.185		
					post (22-27s)	7.12	0.196	0.245	0.0057
			OFF response	10-sec period	pre (70-80s)	6.55	0.224		
					post (82-92s)	5.99	0.200	-0.560	0.0001
				5-sec period	pre (75-80s)	6.46	0.224		
					post (82-87s)	6.09	0.204	-0.373	0.0004

Table S2

Strain	Genotype	Note
N2	*C. elegans* wild-type	Figure 1A,1B, 2A, 2B, 6A, 6B, 6E, S2A, S2B, S6
	egl-4(ky185)	Figure 1A,1B, 2A, 2B, 6A, 6B, 6E, S2A, S2B, S6
	egl-4(n478)	Figure 1A
FK311	*ceh-36(ks86)*	Figure S6
QD 65	*egl-4(ky185); ceh-36(ks86)*	Figure S6
QD 66	*ttx-3(ks5)*	Figure S2A, S2B
QD 67	*egl-4(ky185); ttx-3(ks5)*	Figure S2A, S2B
QD121	*egl-4(ky185); ttx-3(ks5); Ex[trimmed ttx-3p::ttx-3/myo-3::gfp]*	For TTX-3 rescueing experiment, Figure S2B
JN578	*pels578[npr-9p::casp1/npr-9p::venus/unc-122p::mCherry]*	AIB(-), Figure 2B
QD 68	*egl-4(ky185); pels578[npr-9p::casp1/npr-9p::venus/unc-122p::mCherry]*	egl-4; AIB(-), Figure 2B
JN580	*pels580[ins-1(short)p::casp1/ins-1(short)p::venus/unc-122p::gfp]*	AIA(-), Figure 2A
QD 69	*egl-4(ky185); pels580[ins-1(short)p::casp1/ins-1(short)p::venus/unc-122p::gfp]*	egl-4; AIA(-), Figure 2A
QD 71	*Ex[trimmed ttx-3p::cz::casp3/trimmed ttx-3p::casp3::nz/trimmed ttx-3p::rfp/lin-44p::gfp]*	AIY(-), Figure 2C, 2D
QD 72	*egl-4(ky185); Ex[trimmed ttx-3p::cz::casp3/trimmed ttx-3p::casp3::nz/trimmed ttx-3p::rfp/lin-44p::gfp]*	egl-4; AIY(-), Figure 2C, 2D
QD 86	*egl-4(ky185); Ex[H20p::egl-4.a::gfp(N)/myo-3::gfp]*	For EGL-4 rescueing experiment, Figure 6A
QD 87	*egl-4(ky185); Ex[egl-4ap::egl-4.a/myo-3::gfp]*	For EGL-4 rescueing experiment, Figure 6A
QD 88	*egl-4(ky185); Ex[tax-4p::egl-4.a/myo-3::gfp]*	For EGL-4 rescueing experiment, Figure 6A
QD 89	*egl-4(ky185); Ex[odr-10p::egl-4.a/myo-3::gfp]*	For EGL-4 rescueing experiment, Figure 6A, 6B
QD 90	*egl-4(ky185); Ex[ceh-36p::egl-4.a/myo-3::gfp]*	For EGL-4 rescueing experiment, Figure 6A
QD 91	*egl-4(ky185); Ex[trimmed ttx-3p::egl-4.a/myo-3::gfp]*	For EGL-4 rescueing experiment, Figure 6A
QD 92	*egl-4(ky185); Ex[gpa-4p::egl-4.a/myo-3::gfp]*	For EGL-4 rescueing experiment, Figure 6B
QD 93	*egl-4(ky185); Ex[daf-7p::egl-4.a/myo-3::gfp]*	For EGL-4 rescueing experiment, Figure 6B
QD 95	*egl-4(ky185); Ex[odr-10p::egl-4.a/daf-7p::egl-4.a/myo-3::gfp]*	For EGL-4 rescueing experiment, Figure 6B
QD 96	*egl-4(ky185); Ex[odr-10p::egl-4.a/gcy-10p::egl-4.a/myo-3::gfp]*	For EGL-4 rescueing experiment, Figure 6B
QD 97	*egl-4(ky185); Ex[hsp-16.2p::egl-4.a/myo-3::gfp]*	For EGL-4 rescueing experiment, Figure 6E
QD122	*Ex[odr-10 tagged gfp/ttx-3p::rfp]*	Figure S1B
QD123	*egl-4(ky185);Ex[odr-10 tagged gfp/ttx-3p::rfp]*	Figure S1A, S1B
Imaging lines		
QD 73	*Ex[odr-10p::YC3.6/ lin-44::gfp]*	For AWA imaging, Figure 1C
QD 74	*egl-4(ky185); Ex[odr-10p::YC3.6/ lin-44::gfp]*	For AWA imaging, Figure 1C
QD 75	*Ex[odr-3p::YC3.60/str-2p::egl-13nls-mCherry/lin-44p::RFP]*	For AWC imaging, Figure 1D, 4A
QD 76	*egl-4(ky185); Ex[odr-3p::YC3.60/str-2p::egl-13nls-mCherry/lin-44p::RFP]*	For AWC imaging, Figure 1D, 4A
QD 78	*lin-15; Ex[ttx-3p::YC2.6 / lin-15]*	For AIY imaging, Figure 3A, 3B, 4B, 5A, 6D, S3
QD 79	*egl-4(ky185); lin-15; Ex[ttx-3p::YC2.6 / lin-15]*	For AIY imaging, Figure 3A, 3B, 4B, 5A, 6D, S3
QD 80	*odr-7(ky4); Ex[ttx-3p::YC2.6 / lin-15]*	For AIY imaging, Figure 5C
QD 81	*ceh-36(ks86); Ex[ttx-3p::YC2.6 / lin-15]*	For AIY imaging, Figure 5B
QD 82	*egl-4(ky185); odr-7(ky4); Ex[ttx-3p::YC2.6 / lin-15]*	For AIY imaging, Figure 5C
QD 83	*egl-4(ky185); ceh-36(ks86); Ex[ttx-3p::YC2.6 / lin-15]*	For AIY imaging, Figure 5B
QD 84	*Is[odr-1::mCasp1.mec-4::gfp]; Ex[ttx-3p::YC2.6 / lin-15]*	AWC/B(-) for AIY imaging, Figure S4
QD 85	*egl-4(ky185); Is[odr-1::mCasp1.mec-4::gfp]; Ex[ttx-3p::YC2.6 / lin-15]*	AWC/B(-) for AIY imaging, Figure S4
QD 98	*egl-4(ky185); lin-15; Ex[ttx-3::YC2.6/lin-15]; Ex[gpa-4p::egl-4.a/lin-44::gfp]*	For EGL-4 rescueing experiment of AIY response, Figure 6D
QD 99	*egl-4(ky185); lin-15; Ex[ttx-3::YC2.6/lin-15]; Ex[odr-10p::egl-4.a/lin-44::gfp]*	For EGL-4 rescueing experiment of AIY response, Figure 6D